QED Antenna Showers in Hadron Decays

Giacomo Morgante
Student ID: 30582296

Supervisor: Prof. Peter Skands

School of Physics and Astronomy,
Monash University

Honours Thesis

Abstract

Monte Carlo event generators are a key tool in understanding the physics that occurs in particle colliders. As our detector precision increases, so to does the need for accurate and comprehensive event generators. In this thesis we implement a process for performing a QED shower off of a decaying hadron in VINCIA [1]. We then validate our results through comparisons to PHOTOS [2, 3, 4, 5, 6], which is the current standard for QED radiation in hadron decays as well as to the main PYTHIA [7] shower. Finally, we outline the limitations of these comparisons as well as extensions we would like to make in the future.

Acknowledgements

I want to thank Peter Skands for his supervision, his ability to explain physics concepts, how PYTHIA and VINCIA work as well as his willingness to sit in meetings and help me with debugging have been critical to both the completion of this project and my growth as a physicist. I would also like to thank Fernando Abudinén for his assistance with setting up EVTGEN and enabling me to get comparisons to PHOTOS. Finally I would like to thank the cohort of honours students this year for their support both moral and with understanding physics concepts.

Contents

1 Introduction

Particle colliders, such as the Large Hadron Collider (LHC) at CERN, are the way in which we experimentally test our theories and drive theory forward when trying to understand fundamental particles and the interactions between them. Unfortunately, in collider experiments only the final states of the collision are observable. These final states consist of the products of the more interesting, less understood process which occur before they reach our detectors. Experimentally we are only able to detect final state particles, which consists of mostly leptons and light hadrons, and work backwards reconstructing the process which created them. This reconstruction process is complicated and it can often be difficult to distinguish between a decay mode of interest, such as $J/\Psi \to \pi^+\pi^-$, and unrelated particles that appear like the decay of interest, such as a pair of pions which may look like a J/Ψ decay but where actually created by separate processes. One of the key tools for understanding these intermediate processes are Monte Carlo event generators (MCEG), such as PYTHIA [7], HERWIG [8] and SHERPA [9]. These tools allow us to model intermediate states based on our theoretical understanding of the process we are interested in. MCEG's are used to make sense of experimental results, such as using simulated to data to train classification algorithms to distinguish a process of interest from the background, which may look like the process of interest.

As we move towards higher precision experiments and collect more data the effect of QED radiation in understanding these processes becomes increasingly important [2]. When a particle radiates its momentum changes, keeping track of how these momenta change is crucial in being able to accurately reconstruct these events. The LHCb experiment is an example of where QED radiation of off hadron decays is relevant. The LHCb experiment is located at CERN and is specifically designed to investigate b-physics, the physics of hadrons involving the bottom (beauty) quark, as wells as other heavy hadron interactions such as those involving a charm quark. The goal of the LHCb experiment is to investigate CP violation in these process as well as other beyond the standard model (BSM) physics. An example of a process where this radiation is of interest at the LHCb experiment is the decay $B^0 \to J/\Psi K^{*0}$ with $J/\Psi \to \mu^+\mu^-$ and $K^{*0} \to K^-\pi^+$. As well as being able to distinguish this decay mode from the prompt decay $B^0 \to K^{*0}\mu^+\mu^-$ with $K^{*0} \to K^-\pi^+$.

For our purposes we are concerned with the VINCIA [1] treatment of radiation in hadron decays as well as how it compares to the current standard PHOTOS [2, 3, 4, 5, 6]. PHOTOS is an all purpose QED radiation generator for QED radiation in hadron decays, meaning that it can interface with a generic MCEG to add radiation after the fact. We will be accessing PHOTOS through an interface with EVTGEN [10], which is a MCEG which is specifically designed to model the decay of hadrons.

There are many reasons we want to implement this internally in VINCIA rather than using the already existing external software. Firstly, an internal implementation is simpler and easier to use as it is avoids all of the technical complications that come with interfacing to external software. An internal implementation is also has benefits in being easier to maintain and build upon as we are not reliant on others to fix bugs or add additional features; We have not been able to verify an update to PHOTOS since the publication of Ref. [6] in 2015. There are also benefits in terms of internal code performing better due to it being able to be run in parallel. Finally, we would like to model the radiation as a parton shower, so that we can interleave the QED radiation with the QCD shower that already exists in VINCIA.

2 Theory

2.1 Hadron Decay

We will briefly discuss hadron decay and what hadrons are before we begin in earnest. A hadron is a bound state of quarks, for our purposes we mostly look at mesons which contain a quark and an anti-quark. Due to their nature as non-perturbative bound states we do not have a simple way to describe them using Feynman diagrams unlike elementary particles. The way we capture the non-perturbative structure of hadrons is with form factors. Form factors are calculated from experimental data, since they can not be calculated perturbatively. They describe the structure of the hadron, the way in which it differs from a point particle. The solution to this non-perturbative structure when drawing Feynman diagrams is to describe the hadronic legs in the Feynman diagram as the four-momentum of the hadron,

multiplied by the hadron decay constant associated with that hadron [11]. The hadron decay constant is a special case of a form factor.

The hadrons we are interested exist as unstable resonance states. This means that are generated with a mass, not equal to their nominal mass but on a Breit-Wigner distribution as laid out in Ref. [7]. This distribution is based on the particle width, which is the reciprocal of the average lifetime.

2.2 QED Radiation

2.2.1 Probability of Emission

We are looking at the effects of QED radiation, the emission of a photon from an electrically charged particle. We shall follow the treatment in Ref. [12] and start with the simplest case, a charged scalar particle which experiences some change in its momentum, such as exposure to a magnetic field, and then emits a single photon. We will represent the Born level process with $\mathcal{M}_0(p, p')$.

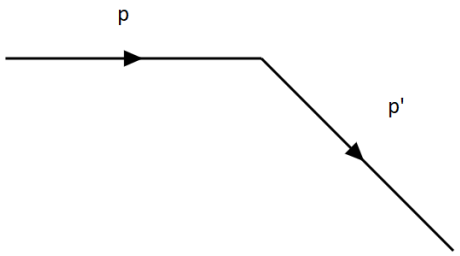

Figure 2.1: The Feynman diagram which illustrates the process associated with the matrix element $\mathcal{M}_0(p, p')$

We can now look at our first order real emission which has two contributing Feynman diagrams, one where the photon is emitted in the initial state and one where it is emitted in the final state.

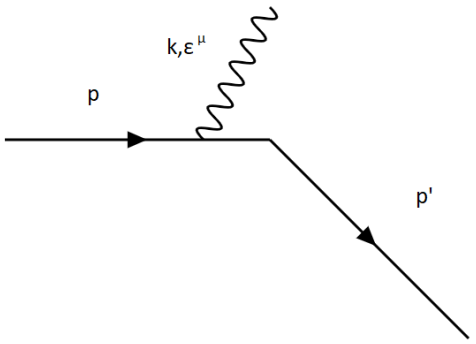

(a) The Feynman diagram which illustrates the process associated with the matrix element $\mathcal{M}_1(p, p')$

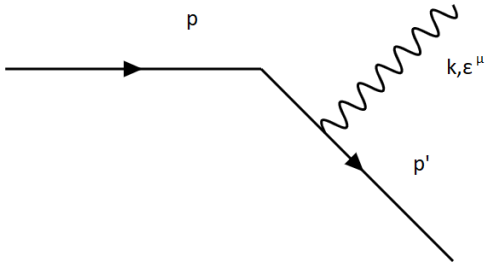

(b) The Feynman diagram which illustrates the process associated with the matrix element $\mathcal{M}_2(p, p')$

Figure 2.2: The Feynman diagrams which illustrates the process associated with the a single photon emission.

With a clear picture of what is going on we can now use these Feynman diagrams to build their corresponding matrix elements.

$$\mathcal{M}_1 = -e\mathcal{M}_0(p-k, p')\frac{i}{(p-k)^2 - m^2}(p+p-k)^\mu \varepsilon^*_\mu(k) \tag{2.2.1}$$

$$\mathcal{M}_2 = e\mathcal{M}_0(p, p' + k)\frac{i}{(p' + k)^2 - m^2}(p' + p' + k)^\mu \varepsilon^*_\mu(k). \tag{2.2.2}$$

We can simplify these matrix elements by choosing to use the Lorenz Gauge, $k^\mu \varepsilon_\mu = 0$ and operating in the soft limit where $|k| \ll |p^0|$. This gives us our matrix elements for a soft photon,

$$\mathcal{M}_1 = -e\mathcal{M}_0(p, p')\frac{p \cdot \varepsilon^*}{p \cdot k} \tag{2.2.3}$$

$$\mathcal{M}_2 = e\mathcal{M}_0(p, p')\frac{p' \cdot \varepsilon^*}{p' \cdot k}. \tag{2.2.4}$$

We can now calculate the total cross section of this process in the usual way by squaring their sum and integrating over the phase space of the photon to get our total cross section for this process,

$$d\sigma(p \to p' + k; \varepsilon) = d\sigma(p \to p') \int \frac{d^3k}{(2\pi)^3 2k} e^2 |\frac{p' \cdot \varepsilon}{p' \cdot k} - \frac{p \cdot \varepsilon}{p \cdot k}|^2. \tag{2.2.5}$$

We call $d\Phi_k$ the phase space element of the photon and use this to calculate the cross section of the process per phase space element

$$\frac{d\sigma(p \to p' + k; \varepsilon)}{d\sigma(p \to p')d\Phi_k} = e^2 \left(\frac{2p \cdot p'}{(p' \cdot k)(p \cdot k)} - \frac{m^2}{(p \cdot k)^2} - \frac{m^2}{(p' \cdot k)^2} \right). \tag{2.2.6}$$

We can already see something that looks like a problem, as $|k| \to 0$, the emitted photon becomes soft, this probability per phase space element will diverge. If we consider the emitting particle to be massless for the sake of simplicity and integrate the right hand size of eq. (2.2.6) over the phase space of the emitted photon we get

$$\begin{aligned} &\int \frac{d^3k}{(2\pi)^3 2k} \frac{2(p \cdot p')}{(p' \cdot k)(p \cdot k)} \\ =&\frac{1}{4\pi^2} \int_0^{k_{max}} \frac{dk}{k} \int_0^1 d\cos(\theta_k) \int_0^{2\pi} \frac{d\phi}{2\pi} \frac{1 - \cos(\theta_{pp'})}{(1 - \cos(\theta_{kp}))(1 - \cos(\theta_{kp'}))}. \end{aligned} \tag{2.2.7}$$

Here we see that we still have the soft divergence we identified in eq. (2.2.5), but we seem to have introduced another divergence as our photon becomes collinear to the emitting particle, θ_{kp} or $\theta kp'$ goes to zero. We can integrate over ϕ so that only our divergences remain giving us

$$\text{Probability of emission} = \frac{e^2}{4\pi} \int_0^{k_{max}} \frac{dk}{k} \int_{\cos(\theta_{pp'})}^1 \frac{d\cos(\theta_k)}{1 - \cos(\theta_k)}. \tag{2.2.8}$$

We need to regulate these divergences and so we introduce k_{min} and θ_{min}, a minimum photon energy and a minimum angle of emission. We can physically motivate these decisions by considering k_{min} to be a photon with a wavelength the size of the universe. In many treatments k_{min} is instead regulated by a fictitious photon mass, θ_{min} is naturally regulated by the mass of the emitting particle as we will see in eq. (2.4.11). Once we have introduced these quantities we can compute our integral to obtain what is known as the Sudakov double logarithm

$$\frac{e^2}{4\pi} \ln\left(\frac{k_{max}}{k_{min}}\right) \ln\left(\frac{1 - \cos(\theta_{pp'})}{1 - \cos(\theta_{min})}\right). \tag{2.2.9}$$

While we have regulated the divergence in that we no longer have an infinite probability, our "probability" can still be greater than one. We can make sense of this by thinking about what we have actually calculated, we have not calculated the probability that we emit one photon but instead we have calculated the average number of photons for the process at first order. More specifically we have calculated the average number of resolvable photons i.e. photons with $k \geq k_{min}$ and $\theta_k \geq \theta_{min}$.

2.2.2 Resolving the Divergence

We still need to deal with the divergence that occurs as k_{min}, $\theta_{min} \to 0$. We have so far neglected the interference between our Born level process and the single virtual photon emission (one loop). The single virtual photon emission and the Born level process are degenerate final states and in quantum mechanics we must sum over degenerate final states as we did to get eq. (2.2.5).

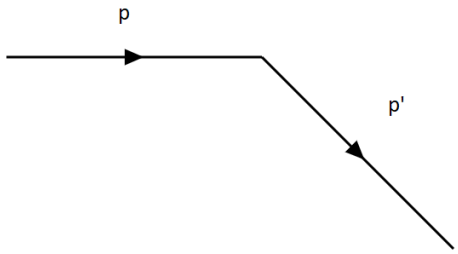

(a) The Feynman diagram for the no emission process

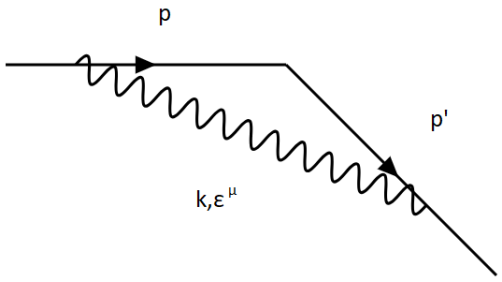

(b) The Feynman diagram for the one virtual emission process.

Figure 2.3: The Feynman diagrams for the no emission process (a) and the one virtual emission process (b). We can see that the final states are the same in both.

To aid in this we will change the notation we used earlier for writing these matrix elements

$$\mathcal{M}_0 \to M_0^{(0)} \tag{2.2.10}$$

$$\mathcal{M}_1 + \mathcal{M}_2 \to M_1^{(0)}. \tag{2.2.11}$$

Here the subscript denotes the number of real emission while the superscript denotes the number of virtual emissions. We can now calculate our full next-to-leading order cross section as

$$\sigma_{NLO} = \int |M_0^{(0)} + M_0^{(1)}|^2 \, d\Phi_0 + \int |M_1^{(0)}|^2 \, d\Phi_1 + \mathcal{O}(\alpha^2) \tag{2.2.12}$$

$$\sigma_{NLO} = \int |M_0^{(0)}|^2 \, d\Phi_n + \int 2Re[M_0^{(0)*} M_0^{(1)}] \, d\Phi_0 + \int |M_1^{(0)}|^2 \, d\Phi_1 + \mathcal{O}(\alpha^2). \tag{2.2.13}$$

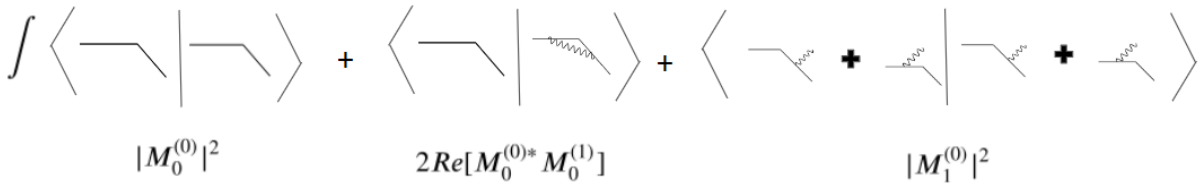

Figure 2.4: The next-to-leading order cross section for a single emission. Here each matrix element has been represented with its corresponding Feynman diagram

What we find is that the interference term ($\int 2Re[M_0^{(0)*} M_0^{(1)}] d\Phi_0$) contains Sudakov double logarithm we found in eq. (2.2.9) for the single real emission term ($\int |M_1^{(0)}|^2 \, d\Phi_1$), however it has the opposite sign and so they cancel each other out and our cross section is no longer divergent. This cancelling of divergences is true to all orders by the Kinoshita-Lee-Nauenberg (KLN) theorem [13]. An explicit demonstration of this cancellation can be found in Ref. [14] for $e^+e^- \to \mu^+\mu^-$.

2.2.3 All Order Corrections

Now that we are confident that we have removed the divergences from our problem at all orders we want to be able to calculate the effects of photon emission to an arbitrary order. We to use the Lorentz invariant form we get in eq. (2.2.6) which we can relate to eq. (2.2.8) in the same way as Larkoski [15].

$$\frac{ds_{a\gamma}}{s_{a\gamma}}\frac{ds_{b\gamma}}{s_{b\gamma}} \propto \frac{dk}{k}\frac{d\theta}{\theta_{a\gamma}} + \frac{dk}{k}\frac{d\theta}{\theta_{b\gamma}} \tag{2.2.14}$$

where s_{ij} is the the dot product of the four momenta of particles i and j i.e. $s_{ij} = 2p_i^\mu p_{j\mu}$, with a and b being a pair of charged particles which can radiate. If we chose to express our Lorentz invariant quantity s_{ij} in a frame dependent we we get $s_{ij} = 2E_iE_j(1-\cos(\theta))$, which we can see goes to zero as the angle between the two particles goes to zero or as either energy becomes zero. In other words it contains both our soft and collinear singularities. Now we can build a recurrence relationship between the differential cross section with n particles and no virtual emissions and the same state with an additional photon as in Ref. [16].

$$d\sigma_{n+1}^{(0)} = g^2\mathcal{N}_{AB\to ab\gamma}(\frac{ds_{a\gamma}}{s_{a\gamma}}\frac{ds_{b\gamma}}{s_{b\gamma}} + \text{less singular terms})d\sigma_n^{(0)}. \tag{2.2.15}$$

Here $\mathcal{N}_{AB\to ab\gamma}$ is a constant and g^2 is the coupling squared. This factorisation of a state with one additional real emission functions is done in the same way that we expressed our matrix elements in eq. (2.2.1) and eq. (2.2.2). When we express this not as a differential cross section but instead as a total cross section we obtain

$$\sigma_{n+m}^{(0)} = \alpha^m(\ln^{2m} + \ln^{2m-1} + \cdots + \ln + \mathcal{R}). \tag{2.2.16}$$

Where $\ln^\lambda$ represents a generic function with transcendentality λ, these functions represent the singular structures. Transcendentality is effectively the number of logarithms that have been multiplied together to create the term, we use a generic measure of transcendentality as occasionally other functions such as dilogarithms can appear. Meanwhile $\mathcal{R}$ is a rational function with transcendentality 0 which is a finite term with no singularity [16]. With this expression the simplest approximation we can make is to ignore all terms but the one with the largest transcendentality. This is known as the double logarithm approximation (DLA) and is the approximation we will be using here for illustration purposes. When using the DLA we can expect to accurately capture the $\ln^{2n}$ and $\ln^{2n-1}$ terms. Since we know that our divergences must cancel to all orders by the aforementioned KLN theorem [13] we know that our virtual emission differntial cross section must be of the same form as eq. (2.2.15) but with the opposite sign.

$$d\sigma_n^{(1)} = -g^2\mathcal{N}_{AB\to ab\gamma}d\sigma_n^{(0)}\int\frac{ds_{a\gamma}}{s_{a\gamma}}\frac{ds_{b\gamma}}{s_{b\gamma}} + \text{less singular terms}. \tag{2.2.17}$$

We now have our two recurrence relations which we can use to perform our corrections to all orders, with our relation corresponding to real emissions acting as a creation operator adding a state with an additional photon and the relation corresponding to the virtual interference acting as an annihilation operator, removing a state which did not emit a photon. This preserves unitarity, so that as we create a state with $n+1$ particles we destroy a state with n particles, keeping our total number of states the same.

2.3 Parton Showers

The parton shower is the way in which we "dress up" a hard process with radiation. The minimum requirements for a parton shower are a radiation function, a phase space factorisation and an ordering variable [7]. We have flexibility in the choices we make for these and the choices we make will be informed by what we want our shower to do best and what trade offs we consider acceptable.

Since we will be working in the DLA we can describe our shower using an iterative Markov Chain, so that each step in our shower only depends on the step before it. We can do this for an arbitrary hard process, F, and an observable $\mathcal{O}$ we can write our differential cross section in terms of $\mathcal{S}$ which we call our evolution operator [16]

$$\frac{d\sigma_F}{d\mathcal{O}}\Big|_{\mathcal{S}} = \int d\Phi_F|M_F^{(0)}|^2\mathcal{S}(\Phi_F,\mathcal{O}). \tag{2.3.1}$$

In defining our evolution operator we need to first define what is known as the Sudakov Factor. The Sudakov Factor is a cumulative distribution function which describes the probability that their is no radiation between two evolution scales. It is way in which we sum over all of our degenerate states [15] and has the general form [16]

$$\Delta(\Phi_n, Q_{E_1}, Q_{E_2}) = \exp\left[-\sum_r \int_{Q_{E_1}}^{Q_{E_2}} \frac{d\Phi^r_{n+1}}{d\Phi_n} S_r(\Phi_{n+1})\right]. \tag{2.3.2}$$

In the Sudakov Factor we sum over all pairs of charged particles which can radiate, r, between our generic evolution scale Q_{E_1} and Q_{E_2} with a phase space factorisation between the current phase space and the phase space of the state after it has radiated, $\frac{d\Phi^r_{n+1}}{d\Phi_n}$ and our radiation function S_r. We will cover the specifics of the Sudakov Factor in the next section however it is worth mentioning it in the context of a familiar process, the decay of a radioactive atom. Where our radiation function is the decay constant, our evolution scales are some initial and final times and the phase space factorisation being replaced with dt and so we can define the "Sudakov Factor" for nuclear decay by

$$\exp[-\int_{t_1}^{t_2} C\ dt]. \tag{2.3.3}$$

With our Sudakov Factor defined we can now define our evolution operator [16],

$$\begin{aligned}\mathcal{S}(\Phi_F, Q_{E_1}, Q_{E_2}, \mathcal{O}) &= \Delta(\Phi_F, Q_{E_1}, Q_{E_2}))\delta(\mathcal{O} - \mathcal{O}(\Phi_F)) \\ &+ \sum_r \int_{Q_{E_2}}^{Q_{E_1}} \frac{d\Phi^r_{F+1}}{d\Phi_F} S_r(\Phi_{F+1})\Delta(\Phi_F, Q_{E_1}, Q_{F+1}))\mathcal{S}(\Phi_{F+1}, Q_{F+1}, Q_{E_2}, \mathcal{O}).\end{aligned} \tag{2.3.4}$$

Here the first line describes all of the terms which do not radiate as we move from our initial evolution scale Q_{E2} to our final evolution scale Q_{E1}. The second line describes the all of the events that did evolve, it also contains the showering operator, which means we have a proper Markov chain.

We have mentioned the evolution scale and ordering variable without elaborating on what that means. The ordering variable defines what one step in our Markov chain is and is the variable which we evolve our shower in. In the case of nuclear decay we mentioned previously the ordering variable is time. The showers we discuss here are ordered in transverse momentum, $p_\perp$. The ordering variable acts as a measure of "softness" or "collinearity" [7] and so the transverse momentum is a good choice since an emission at a low $p_\perp$ can be either soft or collinear or some combination of the two.

While we have been talking about emitting radiation from final state particles (FSR), we can also describe radiation from initial state particles (ISR). ISR occurs before the hard process of interest and works by resolving our shower backwards in our evolution variable, we find two particles in the initial state and look to see if they are the result of a showering [7].

Finally we should discuss the manner in which we try to restore some accuracy that we lose in making approximations such as the DLA or the antenna functions we use in VINCIA. The soft and collinear singularities are universal and are present in all process, however there are less singular and finite terms which we would like to capture where possible. We do this by matching our approximate matrix elements with exact matrix elements that we have calculate to some fixed order. We can do this with programs such as POWHEG [17] and MC@NLO [18]. One of the largest limitations of this however it that we are mostly confined to next-to-leading order corrections.

2.4 The VINCIA Shower

2.4.1 The Dipole Antenna Formalism

The Dipole antenna formalism is based on the idea that particles radiate coherently as dipoles not as individual particles and that we can not determine which particle actually emits the radiation [19]. Since we are looking at QED radiation we can sum over all of these dipoles and capture the full multipole structure of the radiation, though we still only consider a dipole for the purposes of the kinematics [20]. This means we can capture both the collinear and soft singularities inherently in our showering kernel. We can contrast this with the original Dokshitzer-Gribov-Lipatov-Altarelli-Parisi (DGLAP) splitting kernels

used in the main PYTHIA shower, which capture quite well the collinear region of phase space but require additional work to accurately describe all of phase space [7]. Another benefit of using this formalism is that is allows us to interleave the QED shower with the QCD shower, unlike a formalism such as the YFS exponentiation method [21] which does not have this interleaving effect [16]. Additionally, the YFS formalism does not natively account for terms which contain only the collinear singularity.

Before we continue on it is worth laying out the notation to be used as described in Ref. [22].

$$\begin{aligned} s_{ij} &= 2p_i \cdot p_j \\ m_{ij}^2 &= (p_i + p_j)^2 = s_{ij} + m_i^2 + m_j^2. \end{aligned} \tag{2.4.1}$$

The s_{ij} we have defined here is the same s that appears eq. (2.2.14). We will also use lower case subscripts to denote final-state partons and capital subscripts to denote initial-state partons. For example, m_I would be an initial-state mass and m_i would be a post-branching mass.

2.4.2 Antenna Functions

Antenna functions are define using matrix element factorisation, which we have seen previously such as in eq. (2.2.15). We define our antenna function explicitly as in Ref. [23]

$$a_{j,IK}(s_{ij}, s_{jk}, m_i^2, m_j^2, m_k^2) = \frac{|M_3(i,j,k)|^2}{|M_2(I,K)|^2}. \tag{2.4.2}$$

The antenna function describes the ratio between the matrix element of our initial two particle state, $|M_2(I,K)|^2$, and our final state where we have radiated a photon, j, $|M_3(i,j,k)|^2$. The antenna function is our splitting kernel, or in the more general language we used in the previous section, our radiation function, S_r, and can be thought of as the probability density for our branching.

In the same way that we have ISR and FSR, we also have multiple different antenna functions. These are defined by whether the particles which make up the antenna appear in the initial or final state. If both appear in the final state we have a final-final antenna (FF), if both appear in the initial state we have an initial-initial antenna (II) and if one is in the initial and one is in the final we have an initial-final antenna (IF). For our purposes we do not need to concern ourselves with the II antenna as our initial states only contain one particle, the decaying hadron. We can relate these antenna functions together by crossing symmetry, if we have a particle in the final state we can move it to the initial state by changing the sign of its momentum and using that to calculate the matrix element. In the case of our decaying hadron we are not technically using the IF antenna but instead the resonance-final antenna (RF). RF processes involve the decay of some resonance state, such as a top quark or our decaying hadron, which form an antenna with one of its decay products [24]. RF antennae and IF antenna, however have the same form but we differentiate them as they require different implementations in VINCIA.

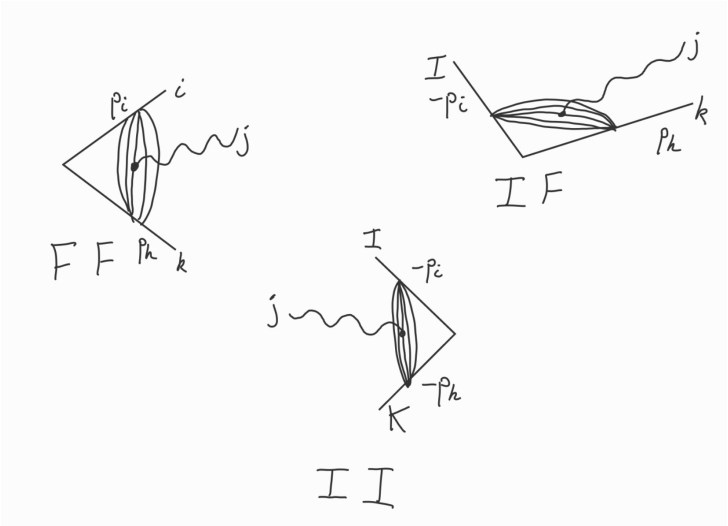

Figure 2.5: The different types of antenna function dipoles II, IF and FF.

2.4.3 Phase Space Factorisation

We have seen in the definition of the Sudakov Factor, eq. (2.3.2) and in section 2.3 that we need a phase space factorisation, a way of relating our pre-branching and post-branching phase space. Since we are using an antenna formalism we will use the antenna phase space factorisation as defined in Ref. [22],

$$\begin{aligned}\Phi_{ik}^{\text{ant}} = \frac{d\Phi_3}{d\Phi_2} =& \frac{1}{16\pi^2}\lambda^{\frac{-1}{2}}(m_{IK}^2, m_I^2, m_K^2) ds_{ij} ds_{jk} \frac{d\phi}{2\pi} \\ & \times \delta(m_{ijk}^2 - s_{ik} - s_{ij} - s_{jk} - m_i^2 - m_j^2 - m_k^2)\Theta(G_{ijk} > 0)\end{aligned} \tag{2.4.3}$$

where λ is the Källén function, $\lambda(m_{IK}^2, m_I^2, m_K^2) = m_{IK}^4 + m_I^4 + m_K^4 - 2m_{IK}^2 m_I^2 - 2m_I^2 m_K^2 - 2m_{IK}^2 m_K^2$, and G_{ijk} is the three-body Gram determinant $G_{ijk} = s_{ij}s_{jk}s_{ik} - s_{ij}^2 m_k^2 - s_{ik}^2 m_j^2 - s_{jk}^2 m_i^2 + 4m_i^2 m_j^2 m_k^2$. The Gram determinant defines whether or not the branching phase space is valid. With this phase space factorisation we can build out the systematic way that we will assign momenta post branching, which is done differently by different showers. In the VINCIA QED and QCD showers both use the same kinematic mapping [25] which is based on massive generalisation of the Kosower [26] mapping.

2.4.4 Sector Antenna Showers

It is worth mentioning briefly that VINCIA is technically a sector antenna shower. This means that while we capture the full multipole structure of the radiation, we only consider one dipole to be radiating instead of tracking all possible histories where each pair may have radiated the photon. The specifics of which are more relevant for the functioning of QCD showers, due to ambiguous decay processes such as $gg \to ggg$, and are detailed in Ref. [23]. They serve to reduce the number of possible shower histories and make performing matrix element corrections less computationally difficult.

2.4.5 The Fully Coherent Shower

VINCIA's fully coherent multipole shower is described in Ref. [22, 20]. When describing the fully coherent multipole shower we first consider the matrix element factorisation in the soft limit

$$|M_{n+1}(\{p\}, p_j)|^2 = -8\pi\alpha \sum_{i,k}^{n} \sigma_i Q_i \sigma_k Q_k \frac{s_{ik}}{s_{ij}s_{jk}} |M_n(\{p\})|^2. \tag{2.4.4}$$

Where Q_i is the charge of particle i, $\{p\}$ is the set of charged particles with momentum, p_j is the momentum of the emitted photon and σ_i is ± 1 depending on whether i is an initial ($\sigma_x = -1$) or final ($\sigma_x = 1$) state particle. When we consider the quasicollinear limit, simply the collinear limit for a massive emitter, we get the following factorisation

$$|M_{n+1}(p_1, \ldots, p_i, \ldots, p_n, p_j)|^2 = 4\pi\alpha Q_i^2 \frac{2}{s_{ij}} P(z, m_i^2, s_{ij}) |M_n(\{p\})|^2. \tag{2.4.5}$$

Where $P(z, m_i^2, s_{ij})$ is the general Altarelli-Parisi (DGLAP) splitting kernel

$$P(z, m_i^2, s_{ij}) = \frac{1 + (1-z)^2}{z} - \frac{2m_i^2}{s_{ij}} \tag{2.4.6}$$

for fermions and

$$P(z, m_i^2, s_{ij}) = 2\frac{z}{1-z} - \frac{2m_i^2}{s_{ij}} + \frac{4}{3}\left(\frac{1-z}{z} + z(1-z)\right) \tag{2.4.7}$$

for the $W^{\pm}$ boson, where z is the energy fraction $z = E_i/E_{i+j}$. For our purposes we treat all spin-one hadrons as if they are $W^{\pm}$ bosons. We can now build our full emission kernels for both FF and IF/RF radiation.

$$
\begin{aligned}
a^{FF}(s_{ij},s_{jk},s_{ik}) = 4\frac{s_{ik}}{s_{ij}s_{jk}} - 4\frac{m_i^2}{s_{ij}^2} - 4\frac{m_k^2}{s_{jk}^2} + \\
\delta_{\text{i is spin-half}}\frac{2}{s_{IK}}\frac{s_{jk}}{s_{ij}} + \delta_{\text{k is spin-half}}\frac{2}{s_{IK}}\frac{s_{ij}}{s_{jk}} \\
\delta_{\text{i is spin-one}}\frac{8}{3}\frac{1}{s_{ij}}\left(\frac{s_{jk}}{s_{IK}-s_{jk}} + \frac{s_{jk}(s_{IK}-s_{jk})}{s_{IK}^2}\right) + \\
\delta_{\text{k is spin-one}}\frac{8}{3}\frac{1}{s_{jk}}\left(\frac{s_{ij}}{s_{IK}-s_{ij}} + \frac{s_{ij}(s_{IK}-s_{ij})}{s_{IK}^2}\right)
\end{aligned}
\tag{2.4.8}
$$

$$
\begin{aligned}
a^{IF}(s_{ij},s_{jk},s_{ik}) = 4\frac{s_{ik}}{s_{ij}s_{jk}} - 4\frac{m_i^2}{s_{ij}^2} - 4\frac{m_k^2}{s_{jk}^2} + \\
\delta_{\text{i is spin-half}}\frac{2}{s_{IK}}\frac{s_{jk}}{s_{ij}} + \delta_{\text{k is spin-half}}\frac{2}{s_{IK}}\frac{s_{ij}}{s_{jk}} \\
\delta_{\text{i is spin-one}}\frac{8}{3}\frac{1}{s_{ij}}\left(\frac{s_{jk}}{s_{IK}+s_{jk}} + \frac{s_{jk}}{s_{IK}} + \frac{s_{jk}^2}{s_{IK}^2}\right) + \\
\delta_{\text{k is spin-one}}\frac{8}{3}\frac{1}{s_{jk}}\left(\frac{s_{ij}}{s_{ik}+s_{kj}} + \frac{s_{ij}}{s_{IK}+s_{jk}} - \frac{s_{ij}^2}{(s_{IK}+s_{jk})^2}\right)
\end{aligned}
\tag{2.4.9}
$$

The first term in each of this antenna functions is called the eikonal term. The eikonal term contains both the soft and collinear singularities explicitly if we use the frame dependent form of $s_{ij} = 2E_iE_j(1-\cos(\theta_{ij})$. The remaining singular terms in each antenna are dependent of the spin of the radiating particle and only contain a collinear singularity and so we call them the collinear terms. The Kronecker-delta functions check the spin of the particle and add them to the antenna if appropriate. We can see in the eikonal and the mass suppression terms, how the emitter mass regulates the collinear singularity [27], if we go to a frame dependent definition of s_{ij}.

$$
\begin{aligned}
&4\frac{s_{ik}}{s_{ij}s_{jk}} - 4\frac{m_i^2}{s_{ij}^2} - 4\frac{m_k^2}{s_{jk}^2} \rightarrow \\
&\frac{2E_iE_k(1-\cos(\theta_{ik})}{E_iE_j^2E_k(1-\cos(\theta_{ij})(1-\cos(\theta_{jk})} - \frac{m_i^2}{E_i^2E_{j^2}(1-\cos(\theta_{ij})^2} - \frac{m_k^2}{E_k^2E_{j^2}(1-\cos(\theta_{jk})^2}.
\end{aligned}
\tag{2.4.10}
$$

We can perform some algebra to get

$$
\frac{1}{E_j^2}\left(\frac{2}{(1-\cos(\theta_{ij}))(1-\cos(\theta_{jk}))} - \frac{m_i^2}{E_i^2(1-\cos(\theta_{ij})^2} - \frac{m_k^2}{E_k^2(1-\cos(\theta_{jk})^2}\right). \tag{2.4.11}
$$

We can see that as the θ_{ij} or θ_{ik} gets small the negative terms will get larger faster than the positive term with the exact cut off point where the total becomes negative determined by $\frac{m^2}{E^2}$. This creates a "dead cone" below a certain angle where we expect to see no radiation. With our FF and IF antennae defined we can build our full emission antenna,

$$
a_{emit}^{QED}(\{p\},p_j) = -\sum_{\{i,k\}} \sigma_i Q_i \sigma_k Q_k a_{emit}(s_{ij},s_{jk},s_{ik}) \tag{2.4.12}
$$

Here we sum over all pairs of particles which can emit a photon, capturing the full multipole structure. We can now use this to write our matrix element factorisation for the whole shower and enforce the requirement that it be a sector shower

$$
|M_{n+1}(\{p\},p_j)|^2 = a_{emit}^{QED}((\{p\},p_j))4\pi\alpha\sum_{\{ik\}}\Theta((p_\perp^2)_{ik})|M_n(\{p\})|^2. \tag{2.4.13}
$$

Here we turn our shower into a sector shower through the use of the Heaviside function, Θ. This selects the pair of charged particles, i and k, which have the smallest transverse momentum to the emitted photon and chooses them to be the emitting dipole for kinematic purposes.

2.4.6 The Pairing Algorithm

As an alternative to the fully coherent shower, VINCIA also has a shower which uses a dipole approximation for the radiation. This will be interesting to compare to the multipole shower for decays with many charged decay products. It has following matrix element factorisation.

$$|M_{n+1}(\{p\}, p_j)|^2 \approx 4\pi\alpha \sum_{[i,k]}^{n} Q^2_{[i,k]} a_{\text{Emit}}(s_{ik}, s_{ij}, s_{jk}) |M_n(\{p\}_{ik})|^2. \tag{2.4.14}$$

Instead of summing over all possible pairs of particles which could emit it uses the Hungarian Algorithm [28, 29] to find the maximally screened pairs of charges. If it is not possible to pair up every particle then the coherent shower is run on the remaining unpaired particles. While this does not capture the full multipole, it is computationally faster than the fully coherent shower despite the Hungarian algorithm having a time complexity of $\mathcal{O}(n^3)$. Meaning that the time taken scales with the cube of the number of charged particles we need to pair up.

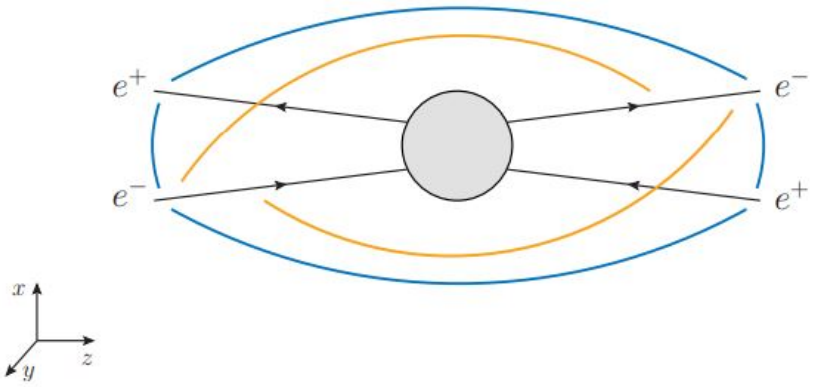

Figure 2.6: A diagram of two electron positron pairs travelling in opposite directions. The blue lines represent a positive antenna while the orange line represents a negative antenna. We can see that the antennas between the far away e^+e^- pairs mostly cancel each other out while the antennas in the nearby pairs dominate [20].

2.4.7 Radiation Below the Hadronisation Scale

In the context of a QED shower for an entire event which starts with a proton-proton collision, we need to change the way we implement radiation due to the confinement effects in QCD when we are dealing with energies below the hadronisation scale. The hadronisation scale is the energy scale at which point coloured partons start forming hadrons and so is naturally of interest to us. The formation of hadrons in PYTHIA and VINCIA is described by the Lund String model [30]. Below the hadronisation scale VINCIA will only shower off of leptons and since the leptons are not necessarily charge conserving will use the colour neutral but electrically charged strings for the purposes of the kinematics. The shower will not account for the electrical charge in the string when deciding whether or not to radiate and does not include any charged hadrons that are present in either the kinematics or the showering [20].

2.5 PHOTOS

For our purposes we are interested in how the QED radiation off of hadron decays is handled in PHOTOS, more specifically PHOTOS++ the C++ implementation of PHOTOS. PHOTOS is not a parton shower but is instead a general purpose after-burner which is intended to interface to a generic Monte Carlo Event Generator and after the decay has occurred generate QED radiation. Based on Ref. [5, 2] it has an exponentiated mode which uses the YFS formalism [21]. While we have been unable to verify the exact implementation used in PHOTOS both HERWIG [31] and SHERPA [32] use this formalism as well and so we will assume that the PHOTOS treatment is functionally similar. This formalism works by expressing the soft divergence using a single coefficient so that as we go to all orders we can exponentiate it.

$$
\begin{aligned}
\mathcal{M}_0^0 &= M_0^0 \\
\mathcal{M}_0^1 &= \alpha B M_0^0 + M_0^1 \\
\mathcal{M}_0^2 &= \frac{(\alpha B)^2}{2!} M_0^0 + \alpha B M_0^1 + M_0^0 \\
\mathcal{M}_0^{n_V} &= \sum_{r=0}^{n_V} M_0^{n_V - r} \frac{(\alpha B)^r}{r!}
\end{aligned}
\tag{2.5.1}
$$

Where $\mathcal{M}_0^{n_V}$, is a matrix element with n_V virtual photons and no real emissions, α is the power of the coupling, $M_0^{n_V}$ is the matrix element with the divergence subtracted out and B contains the divergence as the energy of the photon goes to 0. This generalises to the case with both real and virtual emissions and is described in full in Ref. [21] and succinctly in Ref. [32].

With an exponentiated form containing our divergence we can write the "crude" cross section, which is the cross section based on approximations.

$$
\Gamma_{\text{crude}} = \sum_{n_\gamma=0}^{\infty} \frac{1}{n_\gamma!} \int d\Gamma_0 d\Phi_k e^{Y(\omega)} \prod_{i=1}^{n_\gamma} \tilde{S}_q(k_i) \Theta(k_i, \Omega). \tag{2.5.2}
$$

Here $d\Gamma_0$ is the differential cross section of the born level process, Φ_k is the phase space of the photons, $Y(\omega)$ is the YFS form factor which contains all of the exponentiated divergences, ω is the cut-off for the region defined by Ω, $\Theta(k_i, \Omega)$ partitions the phase space into two regions with the region of phase space defined by Ω containing the divergence in the YFS form factor and then the rest of the phase space which is where we can emit photons, $\Theta(k_i, \Omega) = 1$ if $k_i \notin \Omega$ otherwise it's 0 and $\tilde{S}_q(k_i)$ is the soft divergence term for a photon with momentum k_i which has the form

$$
\tilde{S}(k) = \frac{\alpha}{4\pi^2} \sum_{i<j} \sigma_i Q_i \sigma_j Q_j \left(\frac{p_i}{p_i \cdot k} - \frac{p_j}{p_j \cdot k} \right). \tag{2.5.3}
$$

This sums over all of the dipoles which could emit a photon, with σ and Q having the same definitions as in eq. (2.4.4). We can evaluate the integral in eq. (2.5.2), making the approximation that the YFS form factor $Y \approx -\bar{n}$, the average number of photons we get the final form of the crude cross section

$$
\Gamma_{\text{crude}} = \Gamma_0 \sum_{n_\gamma}^{\infty} \left[\frac{1}{n_\gamma!} e^{-\bar{n}} \bar{n}^{n_\gamma} \right]. \tag{2.5.4}
$$

We can see we now defined our crude cross section as the born level cross section multiplied by a Poissonian distribution with the average number of photon emissions $\bar{n}$. This is used to generate a number of photons, which are then assigned momenta using eq. (2.5.3). Each of PHOTOS, HERWIG and SHERPA then reassign momentum based on their own kinematic remapping schemes. Worth noting is that this formalism does not natively capture the collinear singularity we get in VINCIA from the spin of the particle. These are present but are treated as higher order corrections, in a similar way to the way we consider matrix element corrections in VINCIA.

3 Implementation Overview

Before we go on to make comparisons between VINCIA, PYTHIA and EVTGEN/PHOTOS we should look at how hadron decays were handled before and how we are handling them now. Particle decays in VINCIA/PYTHIA are handled by a decay function. This function handles which decay mode is used, the kinematics of the decay products and importantly for our case it calls the showerQED function. This showerQED function is called exclusively from this decay function and it takes the decay products and builds a system for showering which is then treated like any other system of charged particles. The system is passed to the prepare method in VinciaQED and then after it has been prepared and built we perform the shower from some $p_\perp^2$ scale down to $p_{\perp min}^2$. In section 2.4.7 we discussed how the VINCIA shower has two separate treatments for showering, one for above the hadronisation scale and one for below the hadronisation scale which can only shower off of leptons. While it then seems correct to treat hadron decays using the below the hadronisation scale treatment, and in principle we would like to, lots of the

mechanics of the below hadronisation scale treatment concern strings and the fragmentation process and aren't relevant to many decay processes. This below the hadronisation scale regime was hard coded to only shower off of leptons, since VINCIA was not originally intended to handle hadron decay. We have worked around this restriction by identifying if a system of particles is a hadron decay and then treating it with the full QED multipole shower. This allows us to shower off of hadron decays, without impacting the below the hadronisation scale treatment.

In addition to this more minor changes were made to the surrounding code. The first of which is that the check for whether or not to call the showerQED function was moved from the decay function and instead placed inside the showerQED function itself. This means that each implementation of showerQED can have its own definition of whether or not the function call is valid. Previously the function was only called if the decay was both fully leptonic and had a multiplicity of two. Secondly, the antenna functions that were previously used for the W-boson, now check whether the particle has a SpinType of three and not whether or not it is a W. This allows for the spin of any vector particle to be used in the antenna function; An antenna function was added for spin three halves particles, though it is currently the same as that of the spin half particles and is something to look to implement fully in the future. Finally, switches were made for toggling on and off the individual spin components of the QED shower for both the process level and the hadron decay case.

4 Fully Leptonic Decays

Fully leptonic decays are the simplest decays we can look at and so are the ideal place to start. If we are getting disagreements with the main PYTHIA shower or the results from EVTGEN/PHOTOS then that is a sign that we are doing something wrong. In addition to this comparing e^+e^- final states to $\mu^+\mu^-$ final states is the simplest and clearest way to see if we are handling mass effects as we would expect. We will begin with looking at the VINCIA results by themselves before comparing them first to the main PYTHIA shower and the EVTGEN/PHOTOS results.

4.1 VINCIA Results

We begin by comparing the results of the VINCIA shower for $J/\Psi \to e^+e^-$ and $J/\Psi \to \mu^+\mu^-$. The observables of interest are the total amount of energy radiated by the decay, the opening angle of each radiated photon to the most energetic negatively charged final state particle, which we will refer to as the angular distribution of photons from here and the angular distribution where each entry in the histogram is weighted by the energy of the photon which we will refer to as the energy distribution. The angular distribution and energy distribution are normalised per photon unlike the amount of energy radiated which are per event.

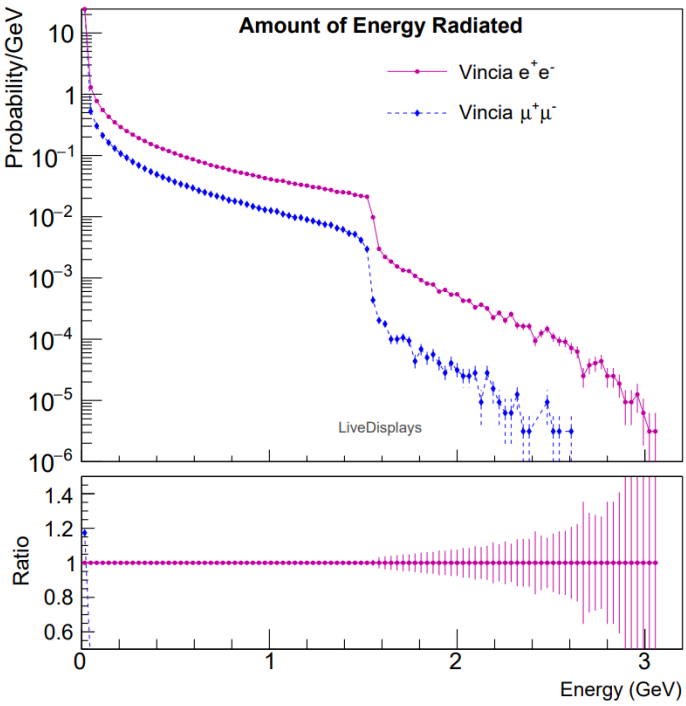

Figure 4.1: The graph of the total amount of energy radiated by the $J/\Psi \to e^+e^-$ (purple) and the $J/\Psi \to \mu^+\mu^-$ (blue).

We can see that the shape of the distribution for both the $J/\Psi \to e^+e^-$ and $J/\Psi \to \mu^+\mu^-$ process is the same, but the decay to muons emits less radiation at each point. This is the expected result as the muon is the same as the electron except for its significantly higher mass. Another place we would expect to see the effect of this mass difference is in the angular distribution of photons.

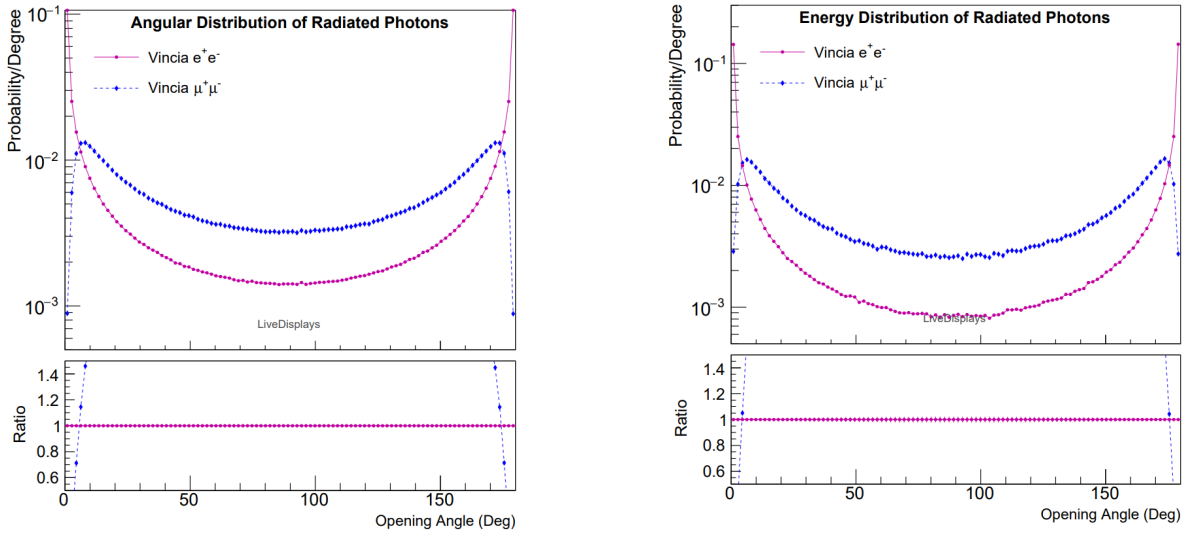

(a) Angular Distribution of Photons.

(b) Energy Distribution of Photons.

Figure 4.2: The graph of the angular distribution of photons for $J/\Psi \to e^+e^-$ (purple) and the $J/\Psi \to \mu^+\mu^-$ (blue) on the top and the energy weighted angular distribution of photons on the bottom.

We can see that the angular distribution in the electron case sees a large enhancement at small angles (small angle to the electron) and at large angles (small angle to the positron), which we would expect as the mass of the electron is small and so we see the enhancement caused by the collinear singularity. Similarly we can see that in the muon decay case we see an enhancement at small and large angles, how-

ever at the smallest and largest angles we see a sharp drop off. We expect to see this as the larger muon mass regulates the collinear singularity and prevents emissions in this region. We can use eq. (2.4.11) to calculate the angle of the dead cone where we expect to see no radiation. We take the energies for each emitting particle to be half the J/Ψ mass and get the respective critical angles.

$J/\Psi \to e^+e^- = 0.83°$
$J/\Psi \to \mu^+\mu^- = 10.85°$

We can not see the effect on the electron state as the angle is less than our bin width, however we see that we are in fact emitting below the angle for the muons. The angle does roughly correspond to where we start seeing the drop off in distribution occur. This is most likely caused by the fact that our angular distribution is calculated based on the angle to the final state particle and not to the particle when the emission occurs. The recoil of the particles for emissions past the first is likely the cause for the emission we see inside the dead cone region. We can see that weighting the angular distribution by the photon energy, seen in fig. 4.2b, changes the shape of the $J/\Psi \to e^+e^-$ decay as well as for the decay to a pair of muons. We see the peak at small angles grow larger for the e^+e^- and correspondingly the trough through the wider angles get lower, indicating that small angle radiation is harder than wide angle radiation. This is again consistent with what we would expect, a hard collinear photon and a soft wide angle photon can both have the same $p_\perp$. Perhaps more interestingly is that we see the same effect in the muon case, where we see that despite seeing proportionally less photons in the region they carry a disproportionate amount of energy

Finally for our final comparison within VINCIA we can look at the effects of turning off the spin terms in the antenna functions.

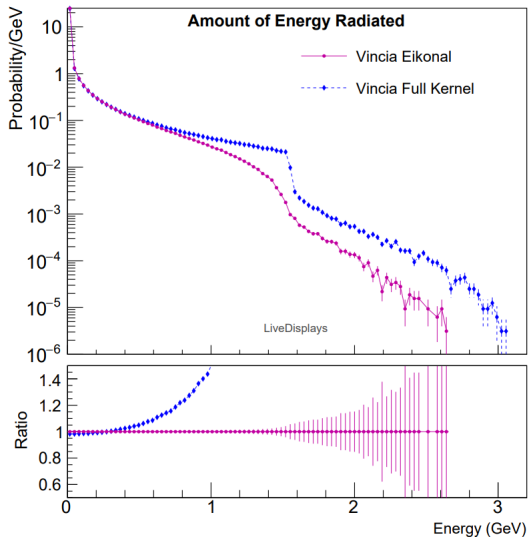

(a) Comparison of energy radiated for $J/\Psi \to e^+e^-$.

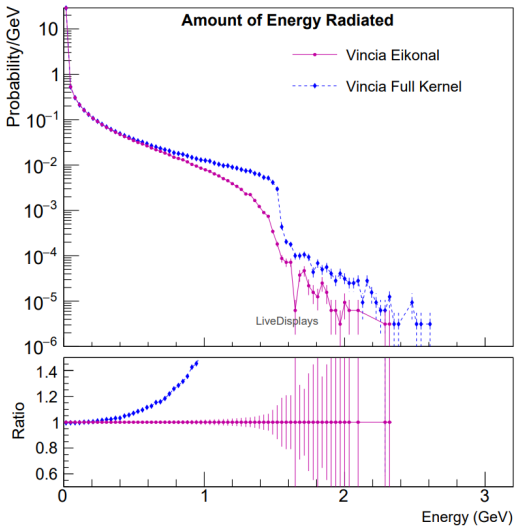

(b) Comparison of energy radiated for $J/\Psi \to \mu^+\mu^-$.

Figure 4.3: The graphs of the total amount of energy radiated VINCIA with the full antenna function (blue) and VINCIA with only the eikonal term (purple).

We can see that turning off the antenna function has the expected effect of decreasing the amount that we radiate in all but the softest regions, where we see proportionally more radiation from the eikonal only graph. We also see that the graph with the eikonal term only has a smaller tail. The difference between the tail of the full kernel and the eikonal term only is greater for the decay to a pair of electrons than to the pair of muons, this is also expected as we can see that the in eq. (2.4.8) and eq. (2.4.9) the eikonal term is depressed by the mass of the emitting particles but won't affect the size of the spin terms. More interestingly is the effect that the spin term, which contains only the collinear singularity, has on the angular distribution of photons and the energy distribution of radiation.

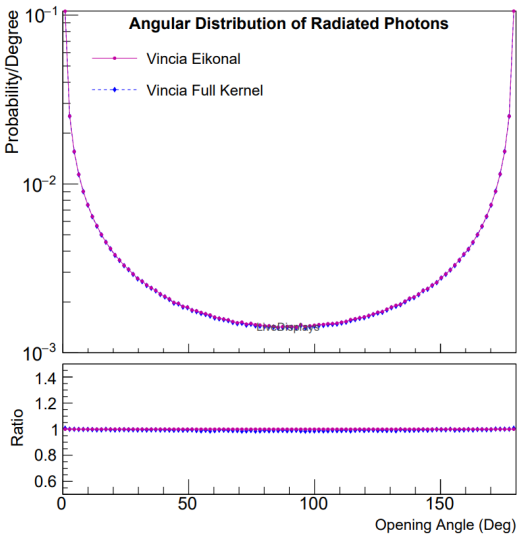

(a) Comparison of angular distribution of photons for $J/\Psi \to e^+e^-$.

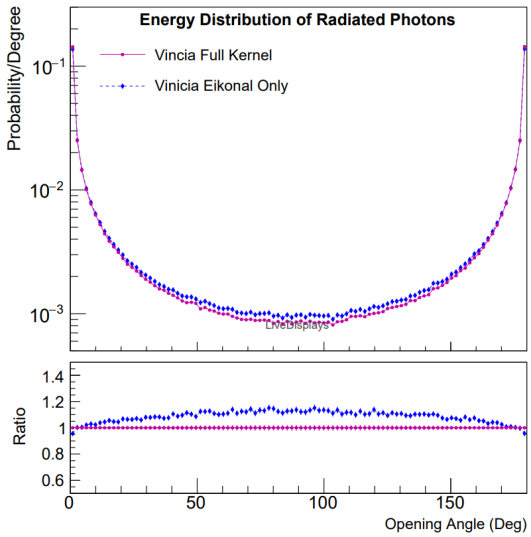

(b) Comparison of energy distribution of photons for $J/\Psi \to e^+e^-$.

Figure 4.4: The graphs of angular distributions for $J/\Psi \to e^+e^-$ VINCIA with the full antenna function (blue) and VINCIA with only the eikonal term (purple).

We see a very small difference in the angular distribution of the radiated photons between the full kernel and eikonal component (fig. 4.4), with the full kernel seeing a stronger enhancement in the collinear region than the eikonal term which makes sense since the extra spin term contains only a collinear singularity. A larger difference is seen in the distribution of the energy (fig. 4.4b), where we see both a stronger enhancement in the collinear regions and correspondingly proportionally less at wide angles.

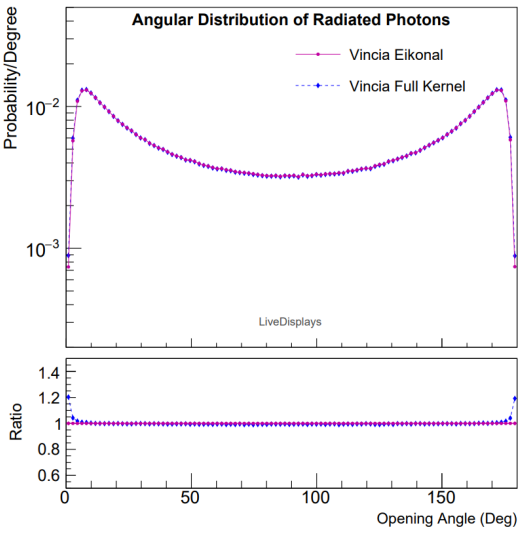

(a) Comparison of angular distribution of photons for $J/\Psi \to \mu^+\mu^-$.

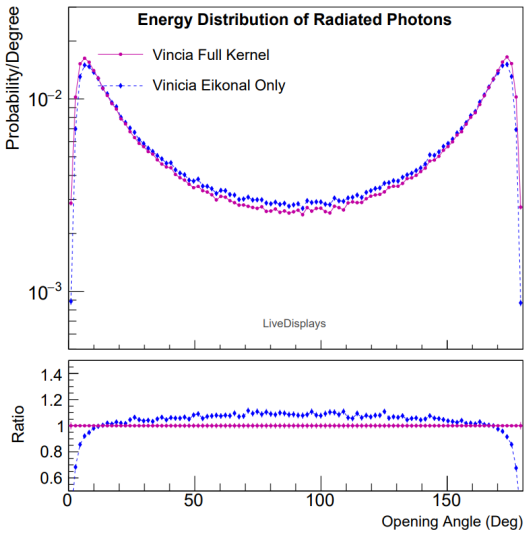

(b) Comparison of energy distribution of photons for $J/\Psi \to \mu^+\mu^-$.

Figure 4.5: The graphs of angular distributions for $J/\Psi \to \mu^+\mu^-$ VINCIA with the full antenna function (blue) and VINCIA with only the eikonal term (purple).

In the same way that we see a stronger enhancement in the collinear region in fig. 4.4a, we also see a small decrease in the suppression of the collinear region for the angular distribution in the full kernel as opposed to the eikonal term only. In a similar way to fig. 4.4b we see a greater proportion of energy radiated in the collinear region and less at wide angles.

4.2 Comparison to PYTHIA

When we compare our observables of interest between the PYTHIA main shower and the VINCIA shower for $J/\Psi \to e^+e^-$ we get the following results.

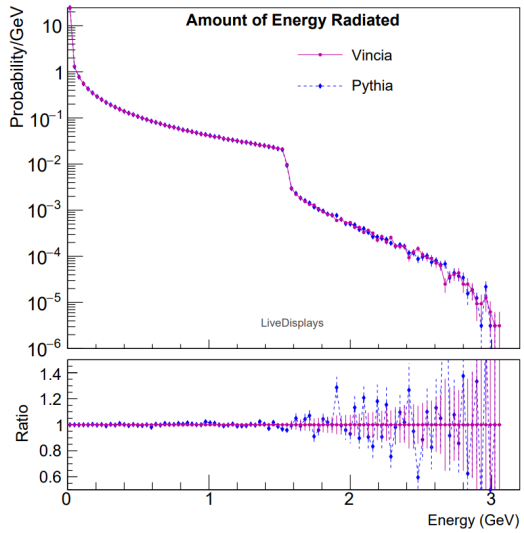

(a) Comparison of energy radiated between PYTHIA and VINCIA.

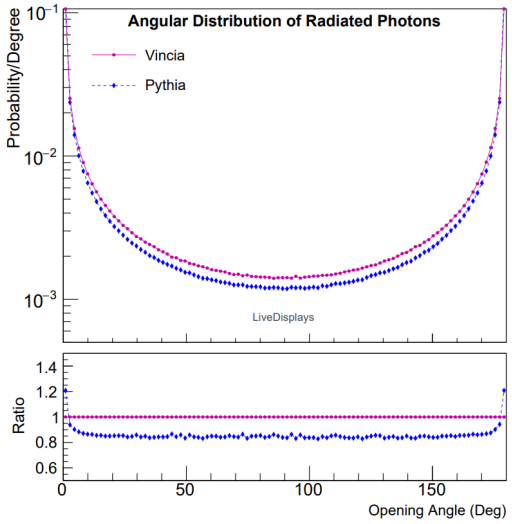

(b) Comparison of the angular distribution of photons between PYTHIA and VINCIA.

Figure 4.6: The graphs of the angular distribution of photons for $J/\Psi \to e^+e^-$ between PYTHIA (blue) and VINCIA (purple).

From this we can clearly see that for the $J/\Psi \to e^+e^-$ case VINCIA and PYTHIA agree on the amount of energy that is radiated, however PYTHIA emits a significantly higher proportion of its photons at the smallest angle to a charged particle, while VINCIA emits proportionally more at larger angles. When we weight the distribution by the energy of the photons as in fig.4.7 we see that this continues, with PYTHIA radiating more of its energy in the collinear region with VINCIA, radiating more at wide angles. Interestingly they seem to radiate a similar amount of energy in the first and last bin, the most collinear region. This is likely due to the fact that PYTHIA uses the DGLAP splitting kernels which describe most accurately the collinear limit. This means that the most collinear region will naturally be more radiative for PYTHIA than VINCIA, however they agree at the smallest angles as the DGLAP splitting will be the term term driving our splitting as we saw in our factorisation in the quasi-collinear limit in eq. (2.4.5).

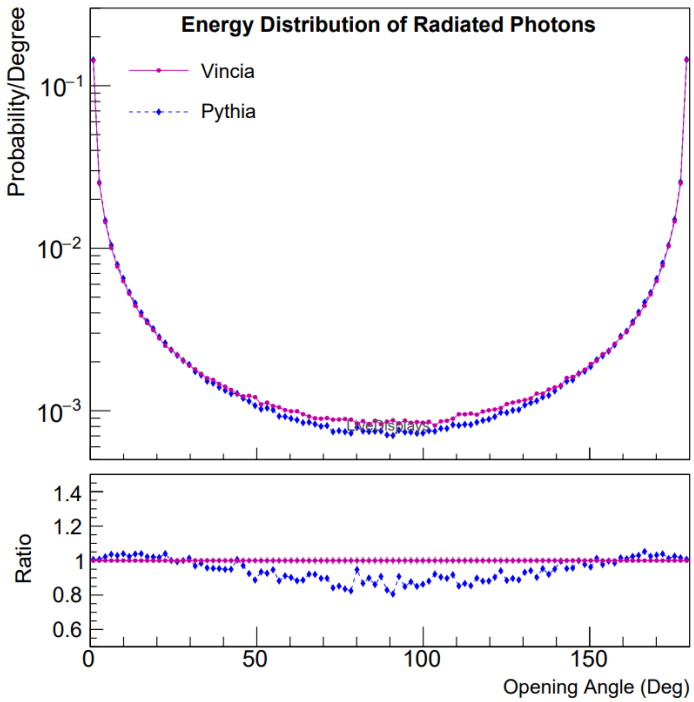

Figure 4.7: The graph of the angular distribution of energy radiated for $J/\Psi \to e^+e^-$ by VINCIA (purple) and PYTHIA (blue).

We can do the same for $J/\Psi \to \mu^+\mu^-$ (fig. 4.8) gives us a very good agreement for events which emit less than 1.5 GeV of energy in the form of radiation. This discrepancy in the greater than 1.5 GeV emitted region of the graph is most likely caused by a lack of events in the region. We believe this as we have seen in the process of obtaining these results that the level of agreement in this region increases with the number of events. The effect on the angular distribution is the same as in the case on the electron positron pair, with PYTHIA radiating proportionally more at the peak enhancement from collinearity and proportionally less at wide angles. We can also see in the ratio pane, that in the most collinear region the PYTHIA shower experiences a higher suppression than VINCIA.

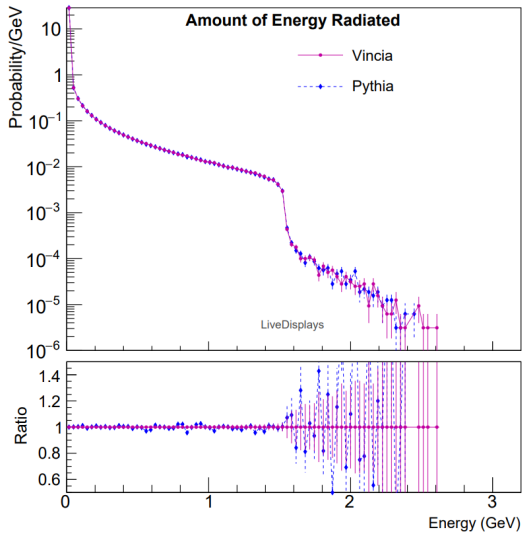

(a) Comparison of energy radiated between PYTHIA and VINCIA.

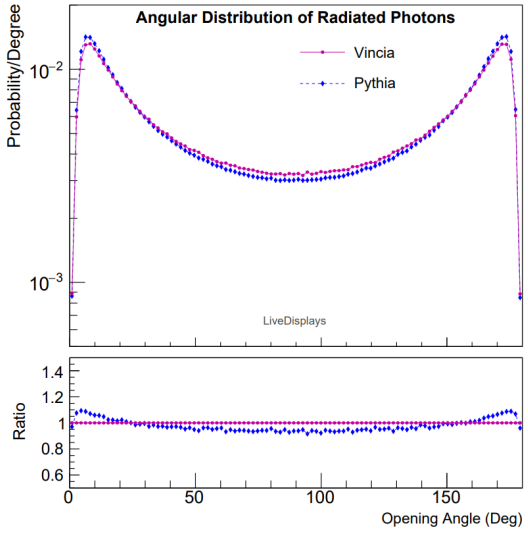

(b) Comparison of the angular distribution of photons between PYTHIA and VINCIA.

Figure 4.8: The graphs of the angular distribution of photons for $J/\Psi \to \mu^+\mu^-$ between PYTHIA (blue) and VINCIA (purple).

When we weight this angular distribution by the photon energy (fig. 4.9) we can see that the discrepancy between the showers in the wide angle region is accentuated and the difference at the most collinear enhanced region is depressed. We also see that despite PYTHIA emitting proportionally less photons in the most collinear region, it radiates a higher proportion of its energy in this region.

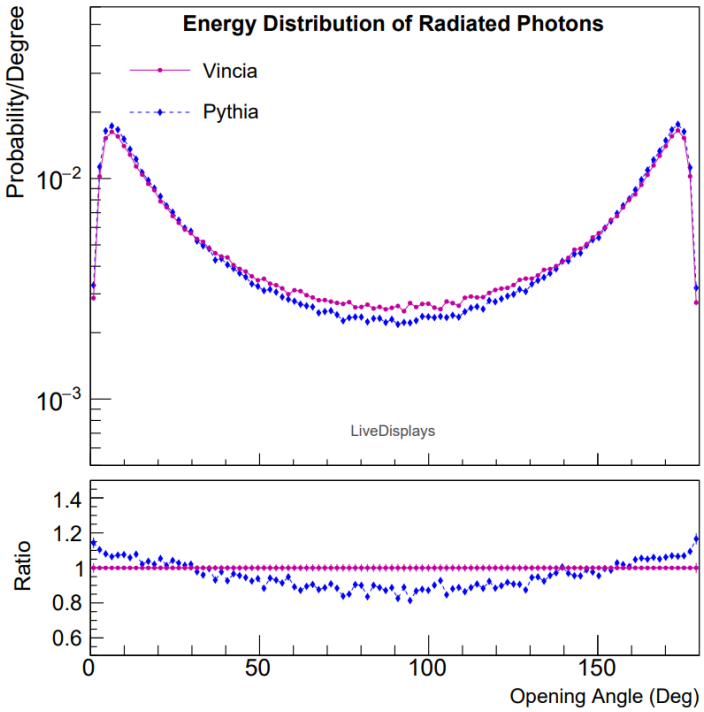

Figure 4.9: The graph of the angular distribution of energy radiated for $J/\Psi \rightarrow \mu^+\mu^-$ by VINCIA (purple) and PYTHIA (blue).

4.3 Comparison to PHOTOS

Comparisons to PHOTOS are what we are most concerned with as it is the current standard for QED radiation in hadron decays. We are doing comparisons to PHOTOS through EVTGEN, this imposes restrictions on the sorts of data we can get and so we will only be looking at comparisons to the total amount of energy radiated.

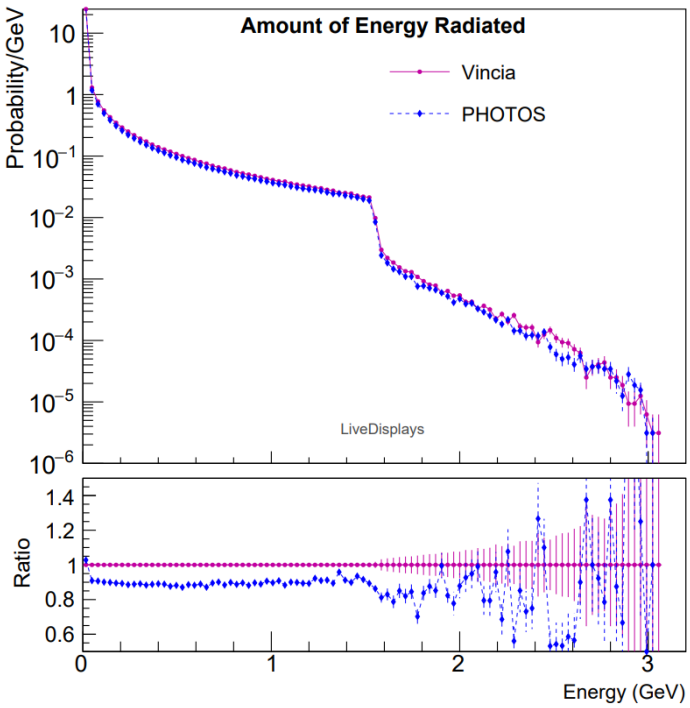

Figure 4.10: Comparison of the total amount of energy radiated between VINCIA (purple) and PHOTOS (blue) for $J/\Psi \to e^+e^-$.

We can see that we have a very good agreement between the radiation produced by PHOTOS and the radiation produced by VINCIA. In the sections of the graph where we have the most statistics PHOTOS radiated around 10% less than VINCIA at all points, except for the peak at zero. The minor difference we see between VINCIA and PHOTOS in the ratio pane in fig.4.10, is indicative of a significant absolute difference in the number of events since the bin value is orders of magnitude larger than any other. This difference seems to be caused by either a larger number of events that don't radiate or a significant number of very soft photons emitted which we look at more in section 5.1.

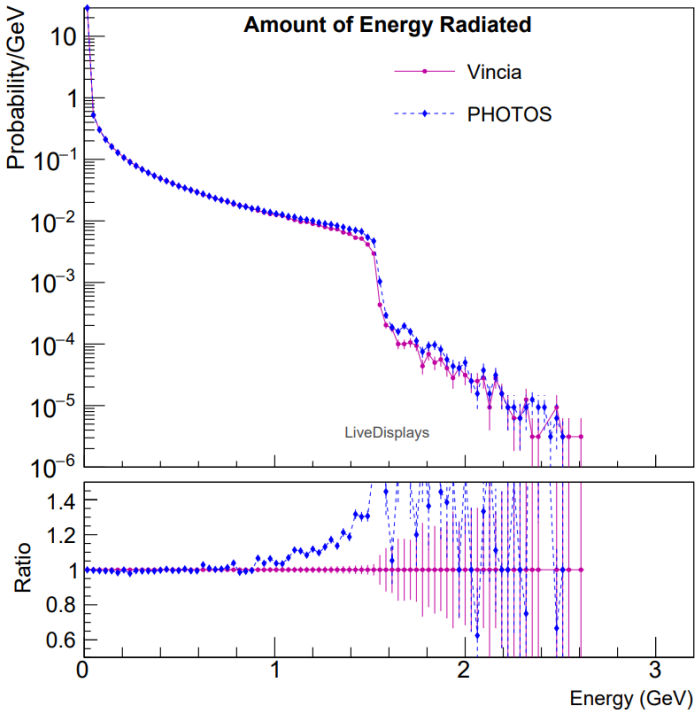

Figure 4.11: Comparison of the total amount of energy radiated between VINCIA (purple) and PHOTOS (blue) for $J/\Psi \to \mu^+\mu^-$.

When looking at $J/\Psi \to \mu^+\mu^-$ (fig.4.11) we don't see the same trend we did in figure 4.10. Instead of VINCIA showering more at almost all points we see near perfect agreement up until around 1GeV, where PHOTOS then starts radiating more than VINCIA. As we go on it is worth keeping this in mind and seeing if there is some relationship between the fraction of the total energy contained in final state masses and where VINCIA radiates more or less than PHOTOS.

5 Technical Subtleties

Now that we have done a preliminary comparison between our showers for the simplest cases, it is worth considering implementation differences that could be affecting the results we see. Specifically in comparison to VINCIA, what is the minimum photon energy we see in PYTHIA and PHOTOS and when comparing to EVTGEN what is the mass distribution of our mother particles and how does that affect our results.

5.1 Infrared Cutoff

Here we would like to look at the effect that our infrared cutoff has on the results we see. As we saw in section 2.2, we still need to introduce some infrared cut off k_{min}. As while our collinear singularities are regulated by the emitter masses, we do not have something equivalent built in for the soft divergence. Experimentally these limits are enforced by the minimum photon energy that we can resolve. Where precisely this cut off is placed varies between the different software we are using and can thus affect the results of observables which are not infrared and collinear safe. An observable is infrared safe if it is unchanged by the addition of a infinitely soft particles, and is collinear safe if it is unchanged by a single particle becoming two comoving particles [16]. While in principle we would like to compare software with identical cutoffs and we would in a more detailed investigation with more time, we can see where these cutoffs lie and keep them in mind when interpreting results. We start by looking at the distribution of the softest photons we see from each generator and comparing that to the number of photons we see emitted.

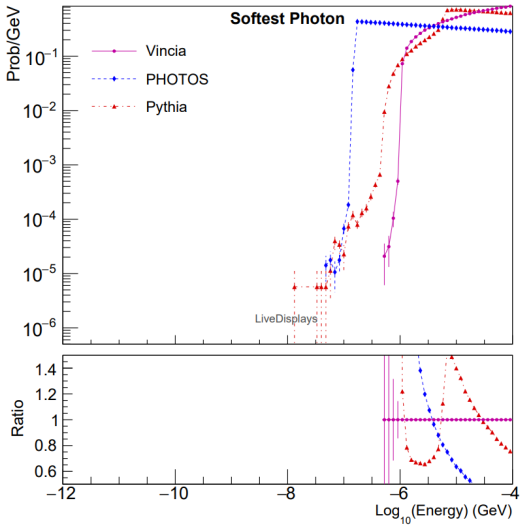

(a) Number of photons emitted of VINCIA, PYTHIA and PHOTOS for $J/\Psi \to e^+e^-$.

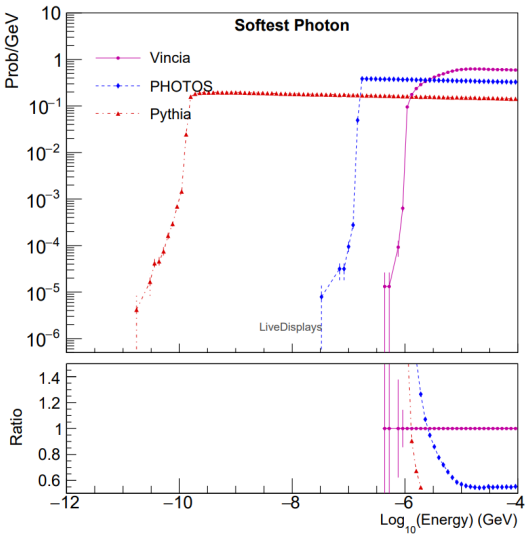

(b) Number of photons emitted in VINCIA, PYTHIA and PHOTOS for $J/\Psi \to \mu^+\mu^-$.

Figure 5.1: The graphs of the softest photons emitted in VINCIA (purple), PYTHIA (red) and PHOTOS (blue).

We can see that both PYTHIA and PHOTOS will emit significantly softer photons than VINCIA. This is particularly notable since PYTHIA and VINCIA should both have a cutoff for photon energy at around 1keV which we do observe in VINCIA but PYTHIA emits significantly softer photons. The softest photon we see in PYTHIA is different for the $J/\Psi \to e^+e^-$ and $J/\Psi \to \mu^+\mu^-$, a full exploration of this is beyond our discussion here, though it is worth noting for future investigation. The fact that PYTHIA is resolving softer photons than VINCIA and emits more photons than VINCIA, yet both emit the same amount of energy clearly demonstrates a fact that is relatively intuitive; The number of photons, and by extension the angular distribution of photons, is not infrared safe and potentially neither is the energy distribution. The infrared unsafe quantities can still give us meaningful information about the differences between our software, we just need to ensure we are careful with drawing our conclusions. These are even more important to keep in mind when comparing infrared unsafe quantities between VINCIA and PHOTOS, as PHOTOS doesn't generate radiation using a parton shower and so the potential for confounding factors is greater.

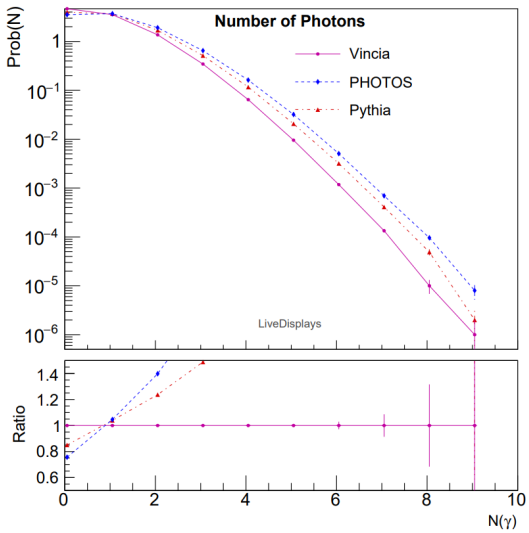

(a) Number of photons emitted of VINCIA, PYTHIA and PHOTOS for $J/\Psi \to e^+e^-$.

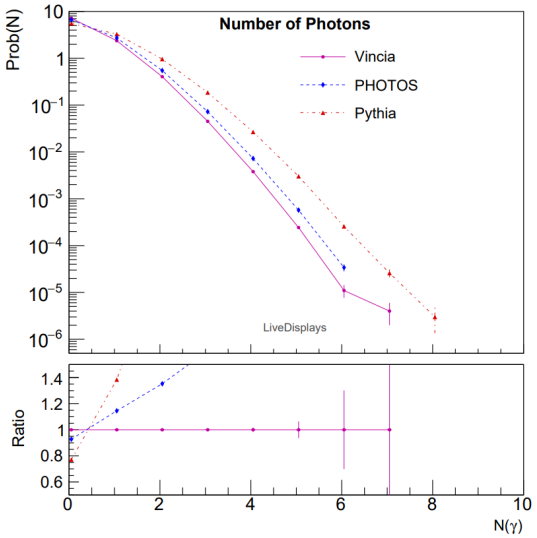

(b) Number of photons emitted in VINCIA, PYTHIA and PHOTOS for $J/\Psi \to \mu^+\mu^-$.

Figure 5.2: The graphs of the number of photons emitted per event in VINCIA (purple), PYTHIA (red) and PHOTOS (blue).

In alignment with this we see that PYTHIA emits the most photons per event and has the least events with no radiation, followed by PHOTOS and finally VINCIA having the most events which don't radiate. This changes how we think about the difference between VINCIA and PHOTOS in figures 4.10 4.11. The significant difference is in the first bin, which we initially believed to be caused by PHOTOS having more events that don't radiate, we can now say that this is most likely caused by PHOTOS radiating lots of events with few photons that are softer than those in VINCIA.

5.2 Mass Distribution

The mass distribution of our mother particles can also contribute significantly to the amount of radiation we see, this is only relevant for comparisons to PHOTOS since VINCIA and PYTHIA use the same system for generating mother particles while we interface to PHOTOS through EVTGEN. The results in sec.4 were created using the default mass distributions for the J/Ψ and so we can graph the mass distributions in each event generator.

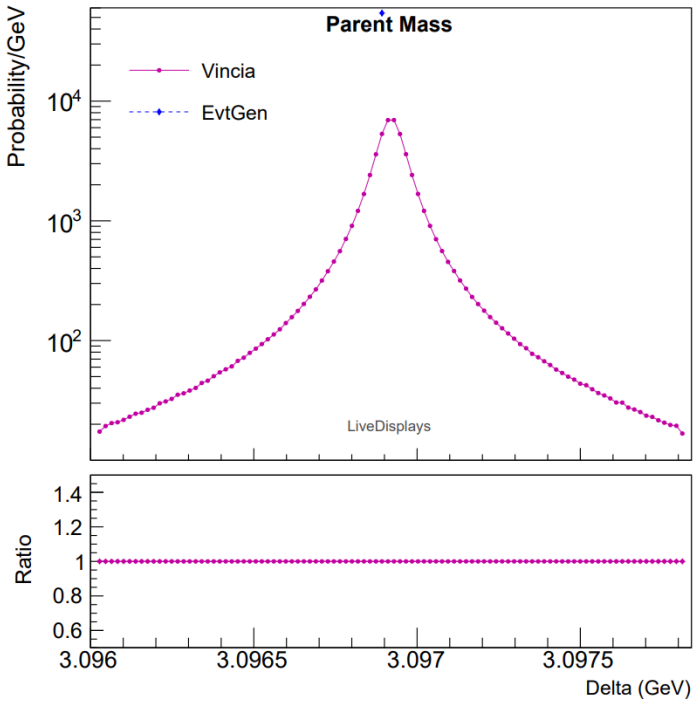

Figure 5.3: The graph of the mass distribution of the J/Ψ in VINCIA and EVTGEN.

We can see that in the case of the J/Ψ, VINCIA generates a symmetric distribution around the nominal J/Ψ mass, whereas EVTGEN seemingly generates all of the J/Ψ's at a value in line with the peak of this distribution. The distribution is quite small with the tails stretching about 1MeV either side of the peak. If we change our Breit-Wigner mode in VINCIA to use the nominal mass of the J/Ψ we get the following graph.

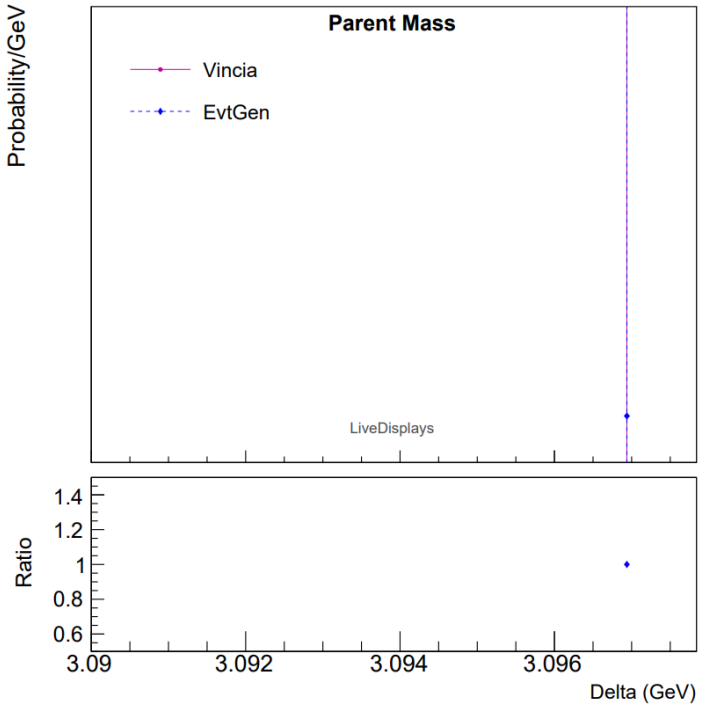

Figure 5.4: The graph of the mass distribution of the J/Ψ in VINCIA with ParticleData:modeBreitWigner = 0 and EVTGEN.

The binning on these two histograms is slightly different, but we can see that all of the J/Ψ's are created in the same bin at the nominal J/Ψ peak. When we look again at the affect this has on the total amount of energy radiated in the $J/\Psi \to e^+e^-$ decay in fig.5.5 we see that this has a negligible affect on the amount of energy radiated.

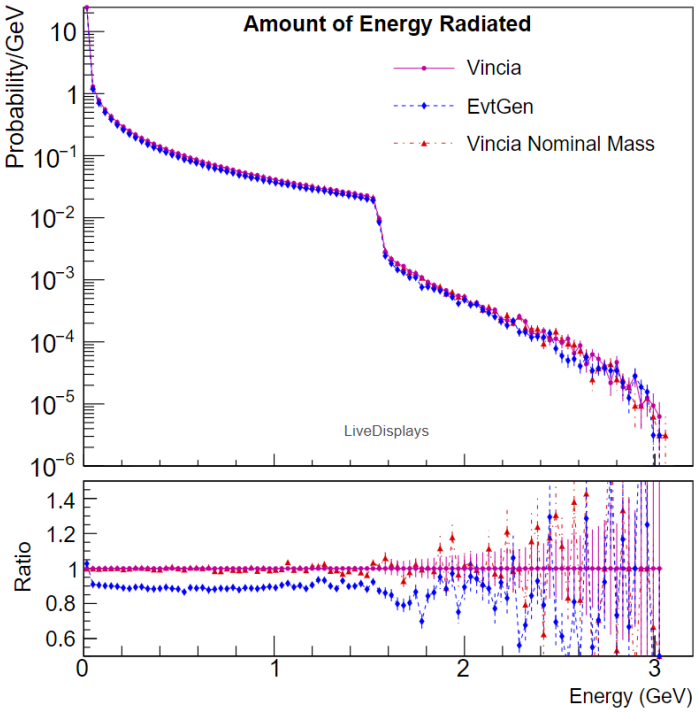

Figure 5.5: The graph of the total amount of energy radiated in PHOTOS/EVTGEN (blue), VINCIA using the nominal J/Ψ mass (red) and standard VINCIA (purple).

With this in mind we can move forward knowing that for hadrons with a small width relative to their nominal mass, such as the J/Ψ which in VINCIA has a nominal mass of 3.09692GeV and a width of 0.00009GeV we can neglect the difference in mass distribution between VINCIA in EVTGEN. We should now consider the mass distribution for particles with larger relative widths such as the ρ whose width is approximately 20% of the nominal mass. When comparing the mass distribution for the ρ^+ meson in EVTGEN with the standard mass distribution of VINCIA we obtain fig. 5.6.

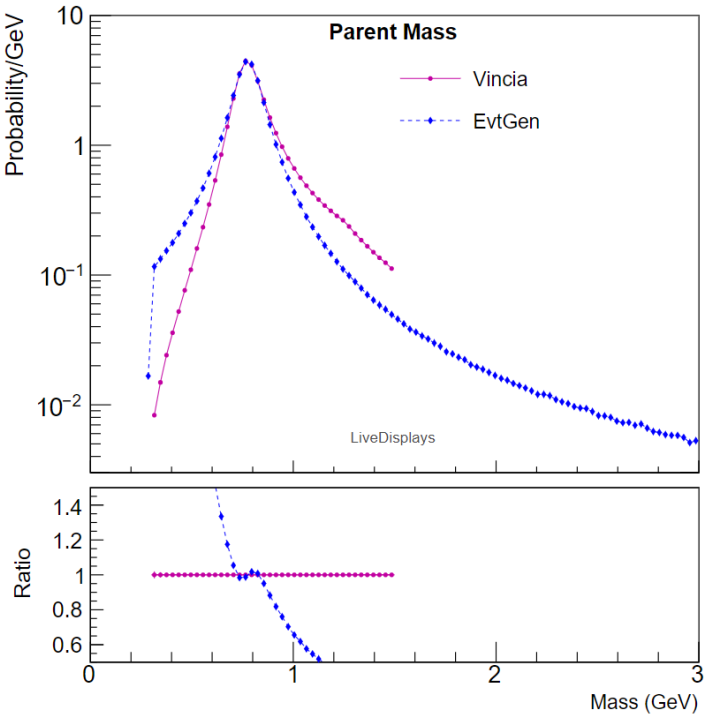

Figure 5.6: Distribution of the ρ^+ mass in VINCIA (purple) and EVTGEN (blue).

We can see that not only do we have a significantly different shape between the two distributions but EVTGEN generates significantly heavier ρ mesons. The total amount of energy radiated per ρ decay will be significantly different with these two distributions as the ρ mesons generated in EVTGEN can radiate far more energy due to the larger mass. We can change the Breit-Wigner mode to change the VINCIA distribution and veto EVTGEN events with masses greater then the largest we see in VINCIA to get fig. 5.7.

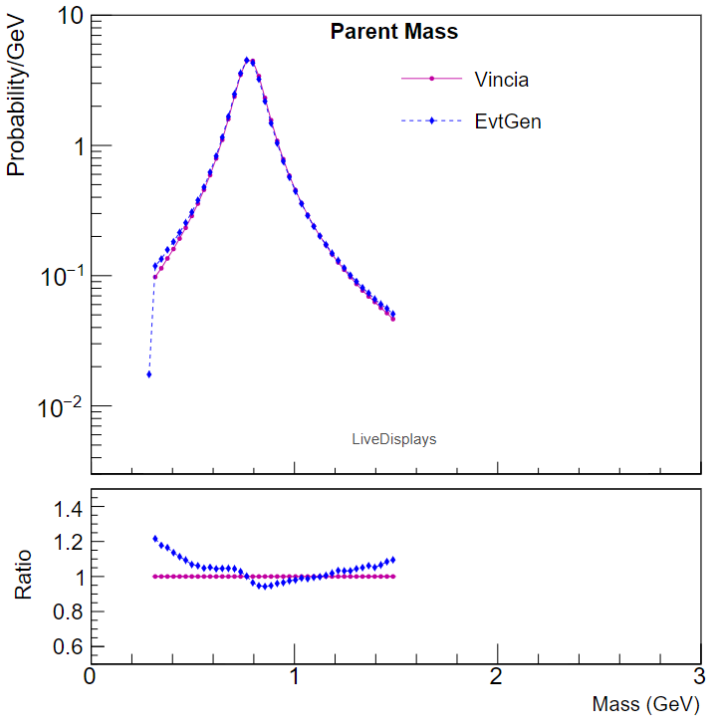

Figure 5.7: Distribution of the ρ^+ mass in VINCIA with ParticleData:modeBreitWigner = 3 mode(purple) and EVTGEN with a veto on any ρ mesons with a mass greater then 1.5GeV (blue).

While we can see that there is still some difference in the mass of the ρ meson the difference is relatively small and should not have a significant effect on results. This is an area where we would like to be able have more control over the way in which we interface with PHOTOS, however we are currently restricted by the structure of EVTGEN.

6 Hadronic Decays

Now we can look at the decay modes which are of the most interest to us, decays with hadronic daughter particles. First we will look at two body decays, before looking at higher multiplicity decays and finally at decays where the incoming hadron is charged. Similarly to the leptonic decays the angular distribution and energy distributions are normalised per photon unlike the amount of energy radiated which are per event.

6.1 Two Body Decays

When looking at two body decays we will look at three decay modes, $D^0 \to \pi^+\pi^-$, $D^0 \to K^+K^-$ and $D^0 \to \pi^+K^-$. This lets us check that we are handling mass effects in our two body hadron decays in the same way that we did in section 4.

6.1.1 VINCIA Results

We start by looking at the amount of energy radiated in these decays in fig. 6.1.

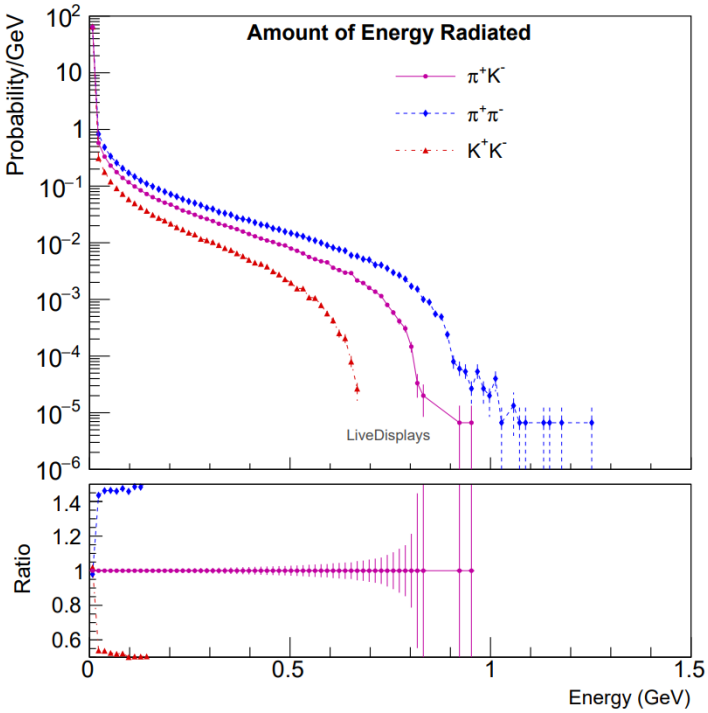

Figure 6.1: The total amount of energy radiated for D^0 decays to $\pi^+\pi^-$ (blue), K^+K^- (red) and π^+K^- (purple).

Here we see the what we would expect, the decay to pions has the largest tail and radiates the most, the decay to kaons has the smallest tail and radiates the least, while the decay to one pion and one kaon sits between them. The decay mode with both a kaon and a pion sits closer to the decay to the pair of pions than it does the pair of kaons.

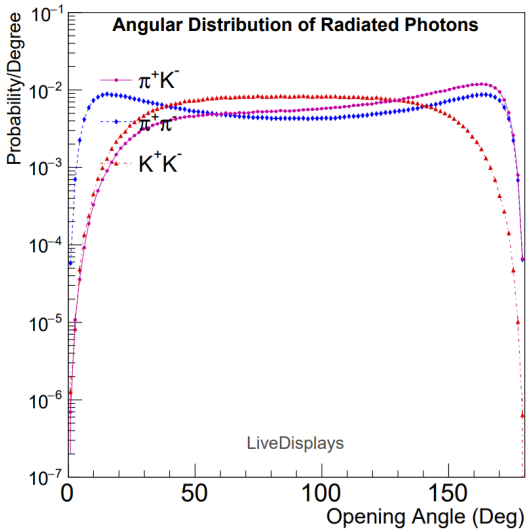

(a) Comparison of angular distribution of photons for D^0 decays to $\pi^+\pi^-$ (blue), K^+K^- (red) and π^+K^- (purple).

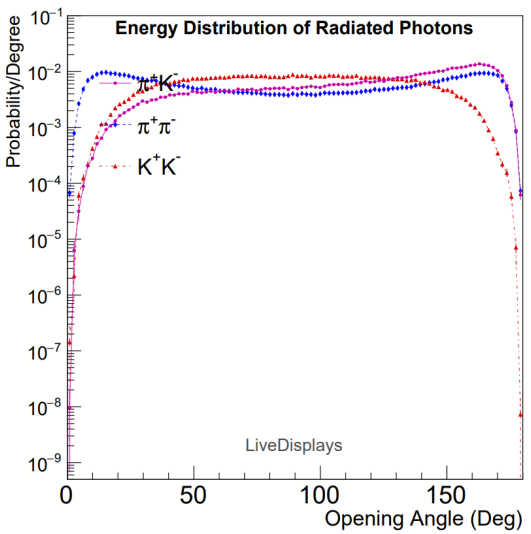

(b) Comparison of energy distribution of photons for D^0 decays to $\pi^+\pi^-$ (blue), K^+K^- (red) and π^+K^- (purple).

Figure 6.2: The graphs of angular distribution of energy for D^0 decays to $\pi^+\pi^-$ (blue), K^+K^- (red) and π^+K^- (purple) in VINCIA.

Here we can see that as we would expect we see a stronger suppression in the collinear region for the more massive K^+K^- final state than the $\pi^+\pi^-$. We also see that the π^+K^-, looks like it has the distribution

of the kaon final state at low angles to the K^- and looks the the distribution of the pion final state at the high angles (low angle to π^+). In both the energy and angular distribution we see that a higher proportion of photons and energy are emitted collinear to the pion, this is also what we would expect as the pion is less massive.

6.1.2 Comparison to PYTHIA

Now that we are confident that our results are internally consistent we can compare to PYTHIA.

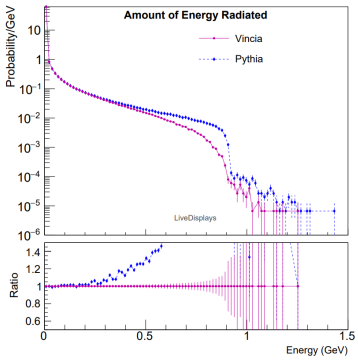

(a) Comparison of total amount of energy radiated for $D^0 \to \pi^+\pi^-$ in VINCIA (purple) and PYTHIA (blue).

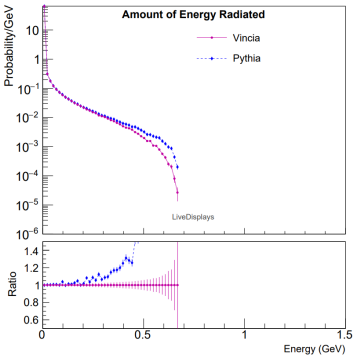

(b) Comparison of total amount of energy radiated for $D^0 \to K^+K^-$ in VINCIA (purple) and PYTHIA (blue).

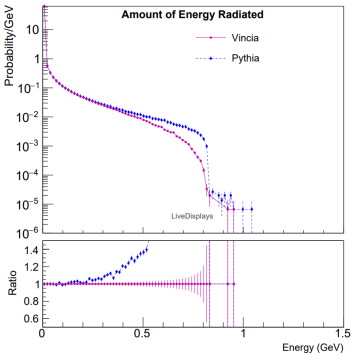

(c) Comparison of total amount of energy radiated for $D^0 \to \pi^+K^-$ in VINCIA (purple) and PYTHIA (blue).

Figure 6.3: The graphs of the total amount of energy radiated for D^0 decays to $\pi^+\pi^-$, K^+K^- and π^+K^- in VINCIA (purple) and PYTHIA (blue).

In all three cases we can see that PYTHIA and VINCIA agree in the soft regions but PYTHIA radiates more at higher energies. PYTHIA also has a slightly larger tail for both modes which contain pions in the final state. We continue to see the difference seems to be mostly affected by the peak in the first bin.

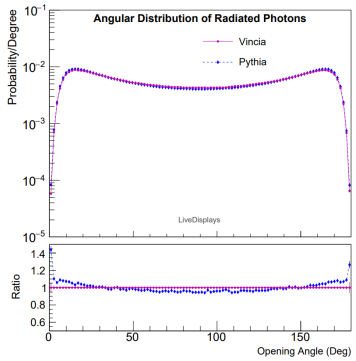

(a) Comparison of the angular distribution of photons for $D^0 \to \pi^+\pi^-$ in VINCIA (purple) and PYTHIA (blue).

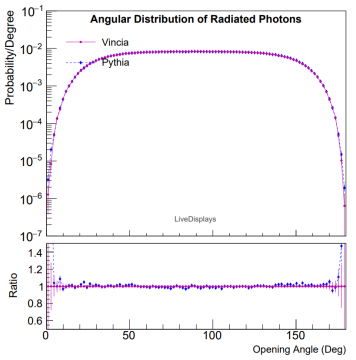

(b) Comparison of the angular distribution of photons for $D^0 \to K^+K^-$ in VINCIA (purple) and PYTHIA (blue).

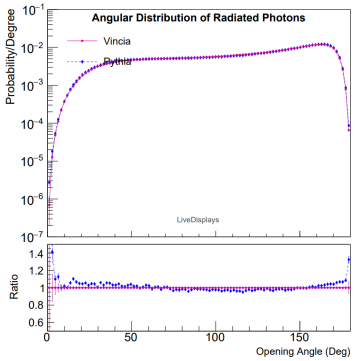

(c) Comparison of the angular distribution of photons for $D^0 \to \pi^+K^-$ in VINCIA (purple) and PYTHIA (blue).

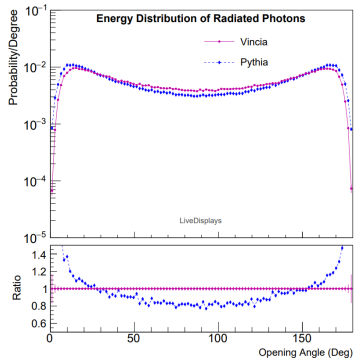

(d) Comparison of the energy distribution for $D^0 \to \pi^+\pi^-$ in VINCIA (purple) and PYTHIA (blue).

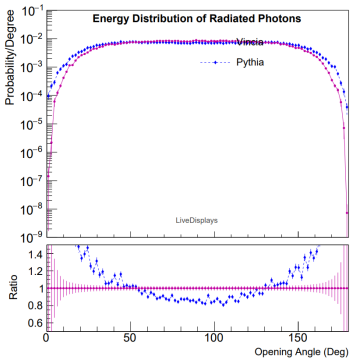

(e) Comparison of the energy distribution for $D^0 \to K^+K^-$ in VINCIA (purple) and PYTHIA (blue).

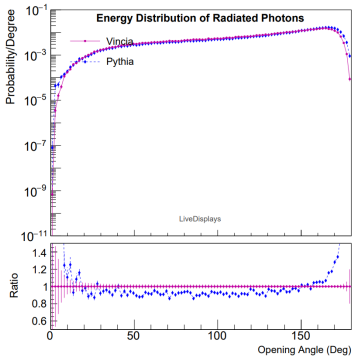

(f) Comparison of the energy distribution for $D^0 \to \pi^+K^-$ in VINCIA (purple) and PYTHIA (blue).

Figure 6.4: The graphs of angular distribution of photons (top row) and energy distribution (bottom row) for D^0 decays to $\pi^+\pi^-$, K^+K^- and π^+K^- in VINCIA (purple) and PYTHIA (blue).

We can see when comparing between the angular distribution with the angular energy distribution we see a similar effect that we saw in section 4.2 where PYTHIA emits a larger portion of its radiation in the most collinear region than VINCIA and this effect is made more pronounced once the energy of the individual photon is considered.

6.1.3 Comparison to Photos

Finally we can compare these decays to the Photos results.

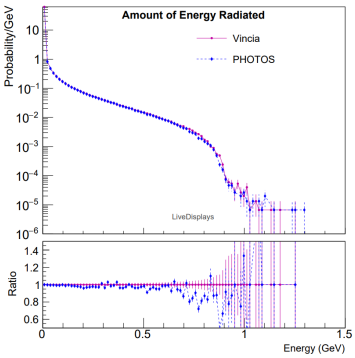

(a) Comparison of total amount of energy radiated for $D^0 \to \pi^+\pi^-$ in VINCIA (purple) and Photos (blue).

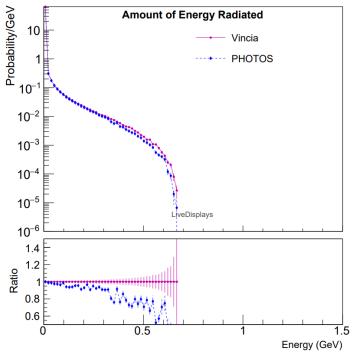

(b) Comparison of total amount of energy radiated for $D^0 \to K^+K^-$ in VINCIA (purple) and Photos (blue).

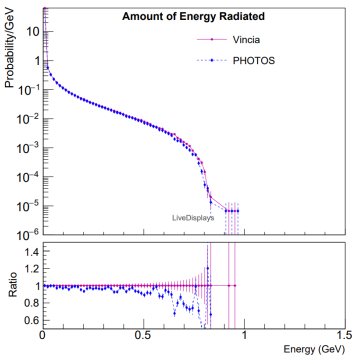

(c) Comparison of total amount of energy radiated for $D^0 \to \pi^+K^-$ in VINCIA (purple) and Photos (blue).

Figure 6.5: The graphs of angular distribution of photons (top row) and energy distribution (bottom row) for D^0 decays to $\pi^+\pi^-$, K^+K^- and π^+K^- in VINCIA (purple) and PYTHIA (blue).

The trend of VINCIA radiating more than Photos in the harder regions continues from what we saw in section 4. Unlike the leptonic case however, where the agreement is better for the heavier muon final state, in the hadronic case we seem to see the opposite effect, where VINCIA seems to start radiating more than Photos sooner for the heavier states.

6.2 Four Body Decays

We want to check that we are consistent in decays with a multiplicity greater than two, however the angular quantities we have been using so far in two body decays do not provide much insight in higher multiplicity decays. This is because the kinematics of a particle at rest to four decay products are far more varied than the simple case of a two body decay where we know what the orientation of the daughter particles must be, so we will just be looking at the amount of energy radiated. These are also the cases where we can really see the effect of the dipole approximation as opposed to the full multipole shower. We only make a comparison between VINCIA's full shower, VINCIA's dipole approximation and PHOTOS because the main PYTHIA shower is hard coded to only treat two body decays.

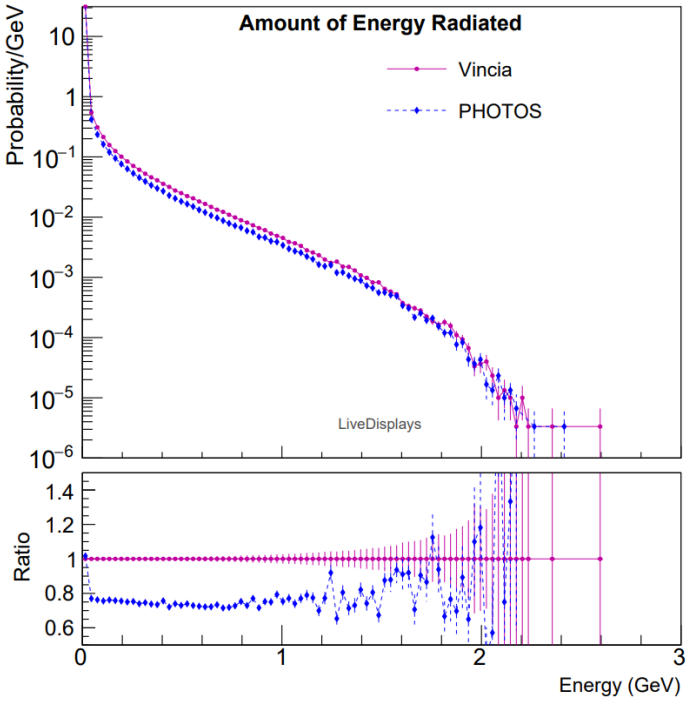

Figure 6.6: The total amount of energy radiated for $B^0 \to K^+K^-\pi^+\pi^-$ in VINCIA (purple) and PHOTOS (blue).

We see a strong agreement between VINCIA and PHOTOS at all points. The trend of VINCIA showering proportionally more outside of the first bin, where PHOTOS is more prominent, continues. We can also use this decay to see the effect of the VINCIA's dipole approximation.

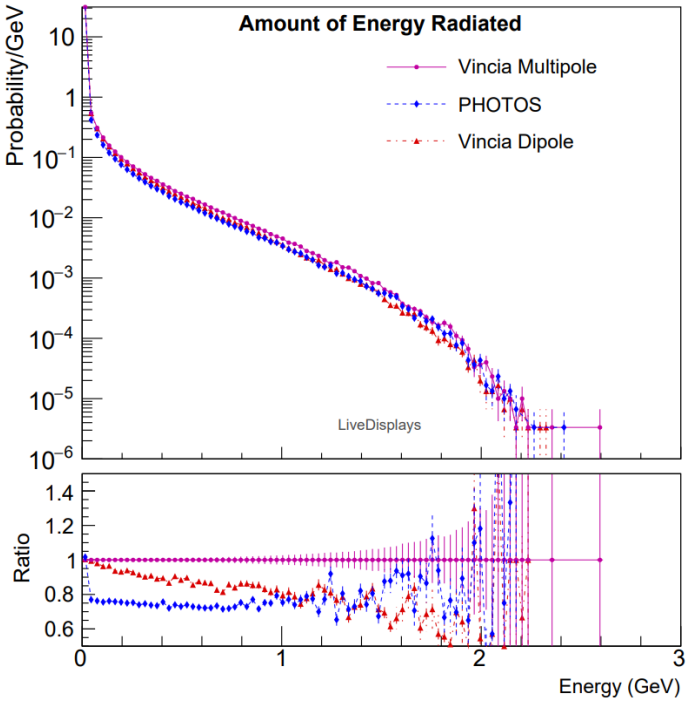

Figure 6.7: The total amount of energy radiated for $B^0 \to K^+K^-\pi^+\pi^-$ in VINCIA's full shower (purple), PHOTOS (blue) and VINCIA's dipole approximation (red).

We can see that the dipole approximation radiates less than VINCIA at higher energies but more than

Photos until past 1GeV Photos takes over. This is interesting and perhaps something to look at in more depth in the future. This effect is potentially caused by the fact that higher energies are likely to require the radiation of more photons and so the difference between the dipole and the multipole becomes more prominent at higher energies, causing PHOTOS to overtake the dipole approximation.

6.3 Charged Initial State

We also need to compare the way that we treat decays where the initial hadron is charged and to that end we will be looking at the decay of $\rho^+ \to \pi^+\pi^0$. As far was we have been able to confirm the specific formalism of an RF antenna is unique to VINCIA and so we would like compare it to the more standard approach.

6.3.1 Comparison to PYTHIA

We start by comparing how the results we get in VINCIA compare to our results from PYTHIA.

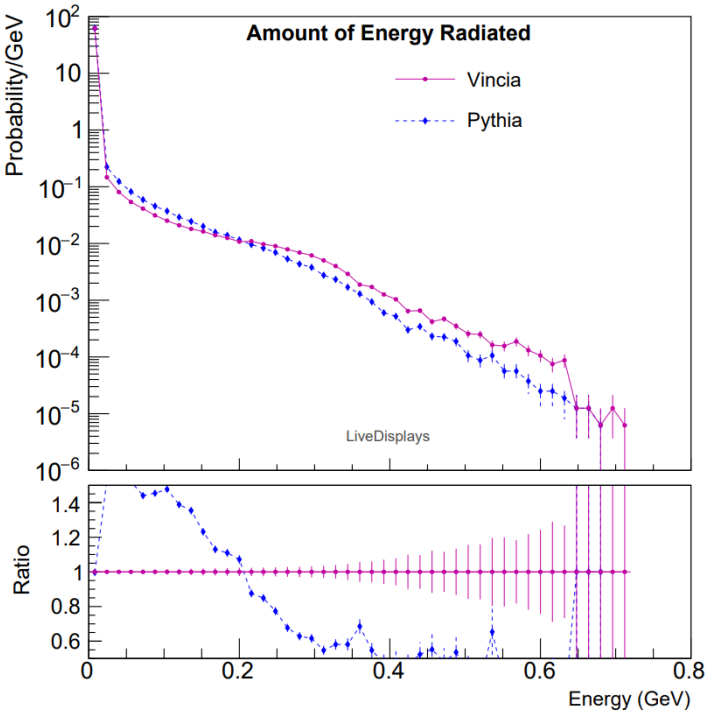

Figure 6.8: The total amount of energy radiated for $\rho^+ \to \pi^+\pi^0$ in VINCIA (purple) and PYTHIA (blue).

We can clearly see that PYTHIA radiates more in the softest regions, before VINCIA starts radiating more in the harder regions. A feature that is somewhat interesting is that excluding the first bin, which contains the events that don't radiate, the line for PYTHIA looks to be linear. As opposed to VINCIA which looks like it would be linear if it weren't for a bump that appears around where the two lines cross and before it then drops off around 0.4GeV. We can now go to look at the angular distributions for this process.

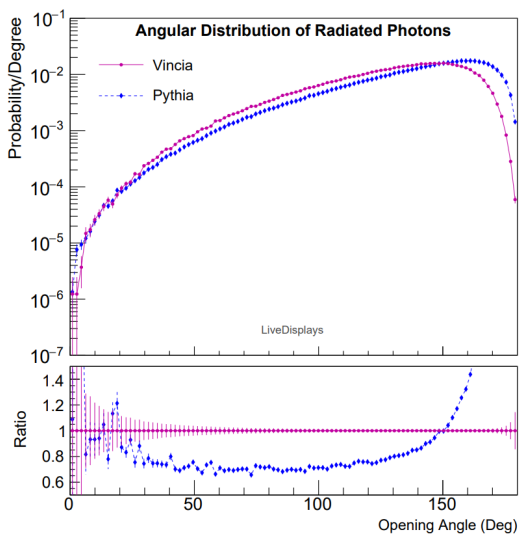

(a) Comparison of angular distribution of photons for $\rho^+ \to \pi^+\pi^-$.

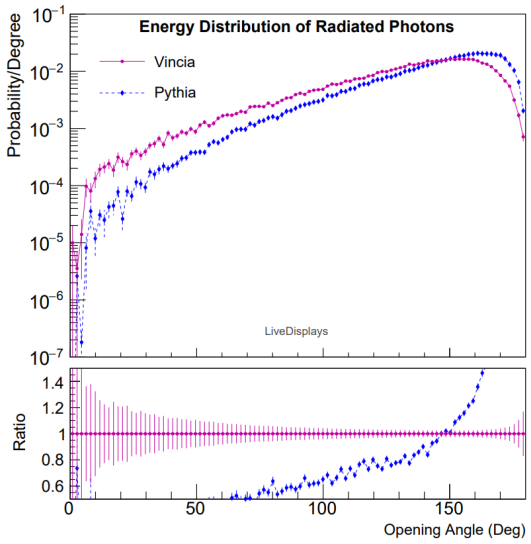

(b) Comparison of energy distribution of photons for $\rho^+ \to \pi^+\pi^-$.

Figure 6.9: The graphs of angular distribution of energy for $\rho^+ \to \pi^+\pi^0$ VINCIA (purple) and PYTHIA (blue).

This graphs both have the general shape that we would expect, with the majority of the events being emitted at a small angle to the π^+ and a steady drop off towards the π^0. We see that PYTHIA emits far more in the most collinear region than VINCIA which is consistent with what we see in figures 4.6b and 4.8b. More interestingly is that when we eight the inputs by their energy we see a similar ratio between VINCIA and PYTHIA at small angles to the π^+, but seemingly much harder radiation in the direction of the π^0 in VINCIA than in PYTHIA. This is consistent with fig. 6.8 where we see VINCIA radiating proportionally more energy than PYTHIA. This gain in the proportion of radiation in the π^0 direction can be thought of as radiation which is collinear to the ρ^+.

6.3.2 Comparison to PHOTOS

We still want to compare the amount of energy radiated in VINCIA with PHOTOS.

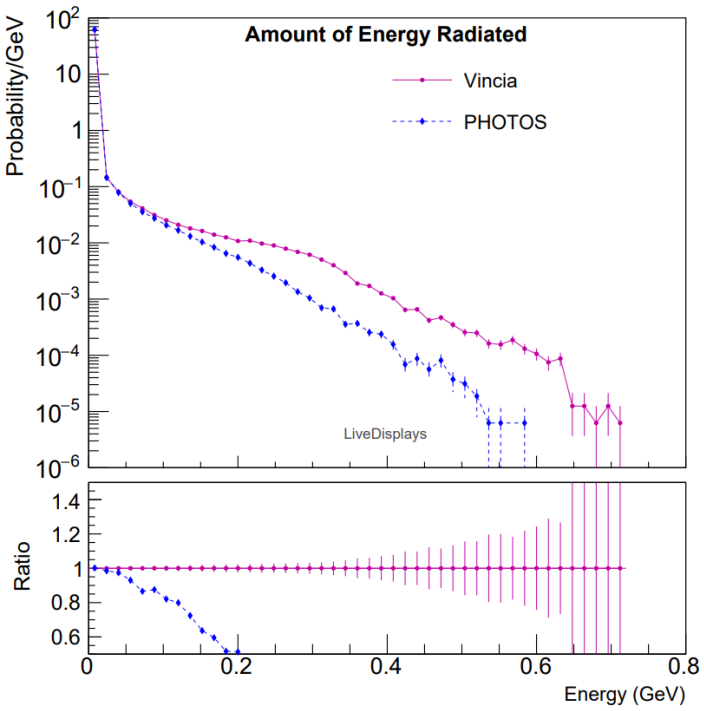

Figure 6.10: The total amount of energy radiated for $\rho^+ \to \pi^+\pi^0$ in VINCIA (purple) and PHOTOS (blue).

Here we see a significant difference between PHOTOS and VINCIA. PHOTOS, like PYTHIA, appears to be linear. Unlike PYTHIA however PHOTOS radiates significantly less than VINCIA at all points except for the softest cases. This level of disagreement is significantly larger than any other we've seen between VINCIA and PHOTOS. We have seen however that the mass distribution for the ρ in EVTGEN and VINCIA is significant even with a veto (fig. 5.7). We can get a measure of this effect by comparing to a different decay to a hadron with a smaller width as compared to its nominal mass, such as the B^+.

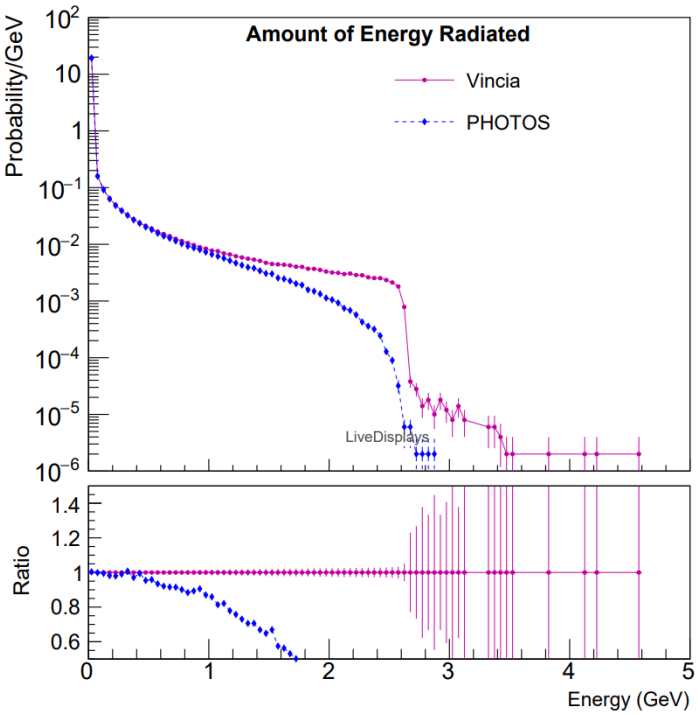

Figure 6.11: The total amount of energy radiated for $B^+ \to \pi^+\pi^0$ in VINCIA (purple) and PHOTOS (blue).

We see a similar effect in the $B+$ decay, a reasonable level of agreement in the softest regions but with VINCIA radiating more at all energies and having a larger tail. This indicates that there is a significant systematic difference between the treatment of charged hadron decays in VINCIA and PHOTOS. This is an area that we would like to explore more in the future, however due to technical limitations we are currently unable perform more comprehensive comparisons. In principle we would like to look at the angular distributions of photons and the energy of individual photons in PHOTOS. Additionally, comparing the PHOTOS treatment of analogous decays that we have a better understanding of how PHOTOS handles the situation such as $W \to \ell\nu_\ell$. In the VINCIA treatment the antenna used in this decay would be similar to a two body decay for a spin one charged hadron, such as the ρ.

6.4 Baryon Decay

So far we have only been comparing the decay of mesons, quark anti-quark bound states, but we should ensure that we see a similar agreement in the decay of baryons, bound states of three quarks.

6.4.1 Comparison to PYTHIA

We start by comparing the amount of radiation emitted between PYTHIA and VINCIA for the decay of $\Lambda_b^0 \to p\pi^-$.

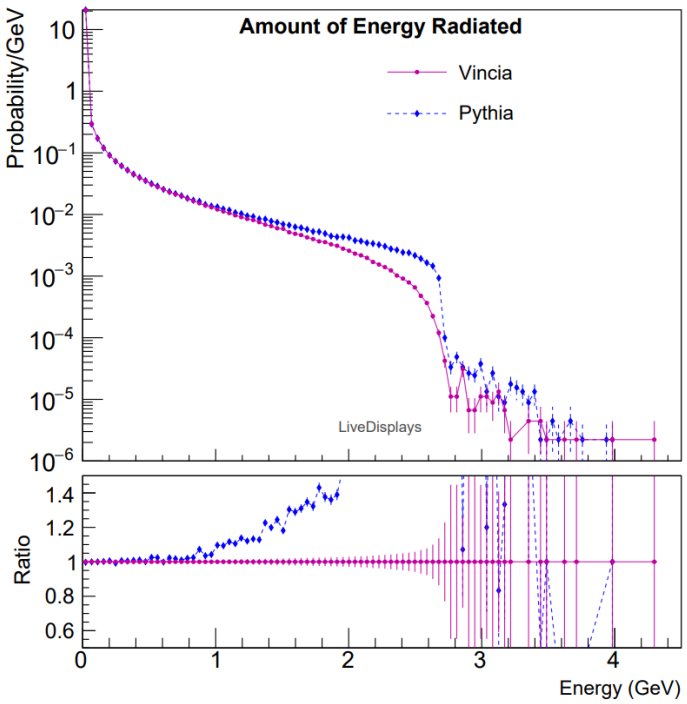

Figure 6.12: The total amount of energy radiated for $\Lambda_b^0 \to p\pi-$ in VINCIA (purple) and PYTHIA (blue).

As with the decays of $D^0 \to \pi^+\pi^-$ in fig. 6.3, we see an agreement in the energy emission events, with PYTHIA radiating proportionally more in the intermediate region before the drop off into the highest region with lacking statistics. The shape of the PYTHIA graph is also very similar in the middle region, with it being flatter with a sharper drop off as opposed to VINCIA which has a smoother drop off.

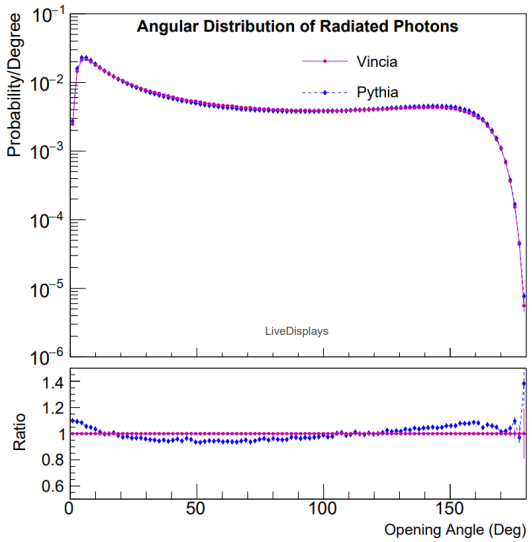

(a) Comparison of angular distribution of photons for $\Lambda_b^0 \to p\pi^-$.

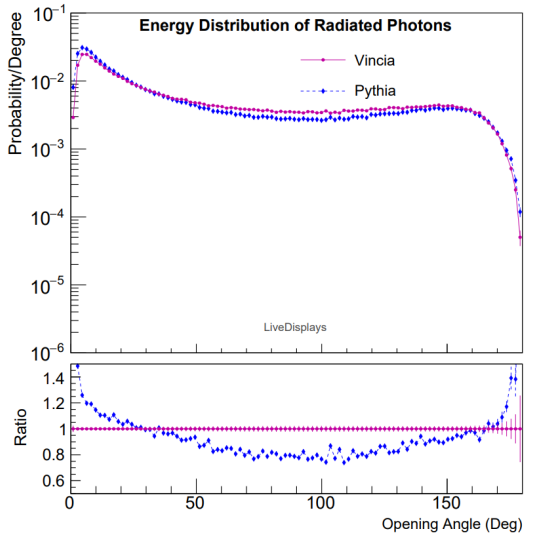

(b) Comparison of energy distribution of photons for $\Lambda_b^0 \to p\pi^-$.

Figure 6.13: The graphs of angular distribution of energy for $\Lambda_b^0 \to p\pi-$ VINCIA (purple) and PYTHIA (blue).

Here we see results consistent with what we would expect, the proton has a larger mass and so experiences a larger suppression, while the lighter π^- experiences less suppression and a relative enhancement. In alignment with previous comparisons, PYTHIA radiates proportionally more at the collinear peaks than

VINCIA. In the energy distribution we again see results consistent with what we have seen so far, with PYTHIA radiating far more energy proportionally in the most collinear regions than VINCIA, while VINCIA radiates proportionally more at wide angles.

6.4.2 Comparison to PHOTOS

When comparing the amount of energy radiated between VINCIA and PHOTOS we see something interesting.

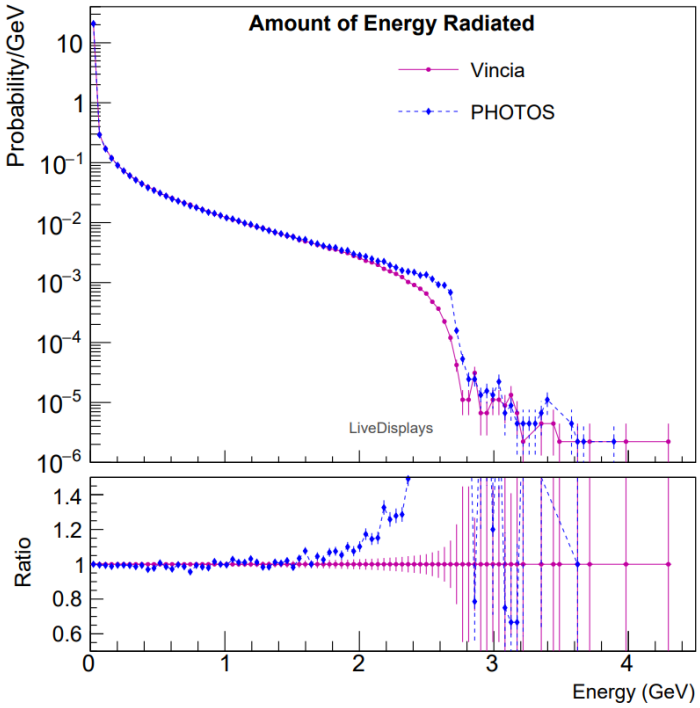

Figure 6.14: The total amount of energy radiated for $\Lambda_b^0 \to p\pi^-$ in VINCIA (purple) and PHOTOS (blue).

While we see very good agreement for much of the graph, this is a case where PHOTOS actually radiates more than VINCIA at higher energies rather than less. We can add the radiation from PYTHIA and see that we still have a greater agreement still in VINCIA.

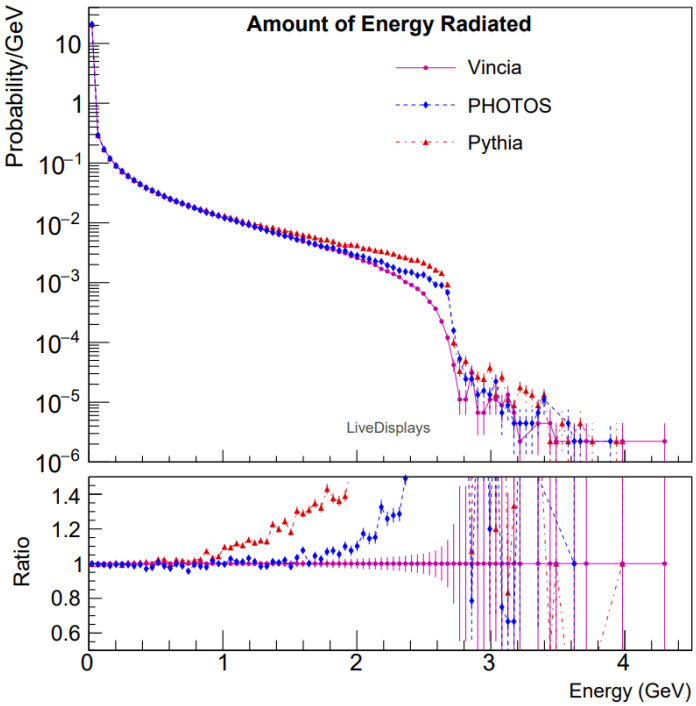

Figure 6.15: The total amount of energy radiated for $\Lambda_b^0 \to p\pi^-$ in VINCIA (purple), PHOTOS (blue) and PYTHIA (red).

We would like to compare an additional baryon decay, to check if this is an anomaly in this specific decay or if it is indicative of a trend in hadron decays. We choose to compare with a similar decay $\Lambda^0 \to p\pi^-$.

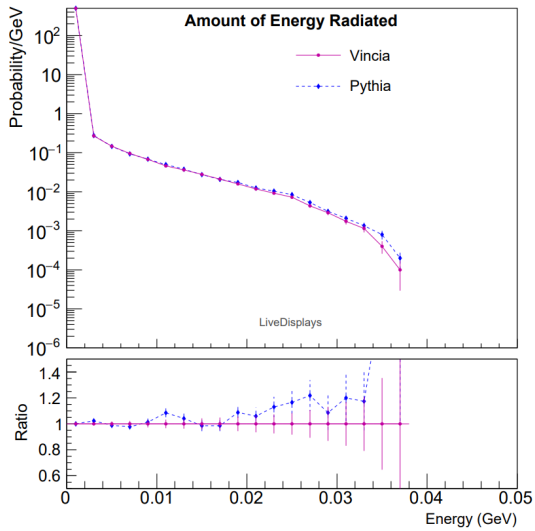

(a) Comparison of the amount of energy radiated for $\Lambda^0 \to p\pi-$ in VINCIA (purple) and PYTHIA (blue).

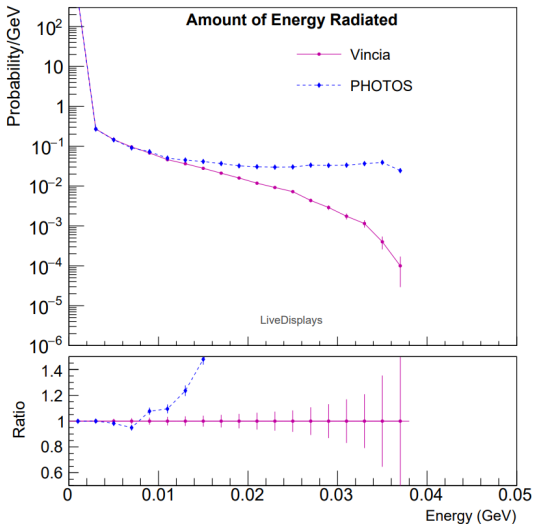

(b) Comparison of the amount of energy radiated photons for $\Lambda^0 \to p\pi-$ in VINCIA (purple) and PHOTOS (blue).

Figure 6.16: The graphs of the amount of energy radiated for $\Lambda^0 \to p\pi-$.

We see as similar effect here as in the other Λ decay and so it seems to be a systematic difference in the way these decays are handled, perhaps owing to the a matrix element correction in PHOTOS which is not present in VINCIA.

7 Future Extensions

While we have a functional implementation for hadron decays there are many avenues for further investigation, both in terms of additions to our treatment and a more thorough comparison with existing software. We have found so far in our comparisons to PHOTOS that VINCIA radiates proportionally more at in all bins outside of the first. With this in mind it would be worth restricting our binning range and looking in this first bin, to better understand what is happening here. Similarly we would like to be able to compare the amount of energy radiated given that the event actually radiated, this would similarly give insight into how technical details, such as the QED cutoff affect our results. Additionally comparing not the absolute amount of energy radiated but instead the fraction of total energy which was radiated, could allow us to see trends that we do not see in the absolute amount of energy radiated. We would also like to run tests where we are directly interfacing with PHOTOS in VINCIA, this will allow us to use different, more physical normalisations for our histograms rather than normalising the area under each histogram to one. This would also allow us to test more observables for PHOTOS such as the angular and energy distributions as we would not be limited by the current EVTGEN environment. Alternatively, we can mitigate some technical factors by using the EVTGEN interface to VINCIA which is under development. Finally, we can investigate the decay of $W^{\pm}$ bosons as being analogous to the decay of a ρ^{+} and see if the differences between radiation off of charged initial states persist. This is an especially good decay to look at as we know that PYTHIA has matrix element corrections implemented for the decay of $W^{\pm}$ bosons.

There are also many ways we would like to build on our current implementation. Firstly, we would like to add an antenna for spin-three-halves particles in a similar way that we have for spin-half and spin-one particles in the antenna functions defined in eq. (2.4.8) and eq. (2.4.9). As mentioned in section 3, while this exists in the code it is identical to the spin-half antenna. In addition, we would like a way to implement form factors in our radiation. As mentioned in section 2.1 the form factor of a hadron describes the way that it varies from point particle. Currently all of our hadrons radiate as if they were point-like and so to really describe the way hadrons radiate having the option to introduce form factors if they are known.

We would also like to implement a fully interleaved decay in a similar manner to that outlined in Ref. [33] for interleaving the electroweak and QCD showers. The goal of interleaved decays in the hadron decay case would be for proper treatment of cascade decays. There are two main cases where we would want this, the first is in the cascade decay of a charged particle where we do not want to go all the way down to the minimum of our $p_{\perp}$ scale then decay the charged particle and use it in an initial shower starting again at the highest $p_{\perp}$, this leads to a double counting and potential over radiation. An interleaved treatment would allow us to shower down to the scale where we would expect the decay to occur and then continue showering of the resonance decay. In a similar case if we decay to two neutral particles we would like to start showering off of the decay products of the shorter lived particle for some period, before we introduce the interference from the decay of the longer lived particle.

While for most decays simply treating the decay using the above the hadronisation scale treatment is accurate, we would like to describe some decay modes using the below the hadronisation scale treatment. An example of such as Λ_c^{+} decays which contain quarks in the final state. A longer term goal may additionally be to consider how an electrically charged string would radiate.

Finally we would like to consider the effect that turning on the QED shower has on the branching ratios of our decays. For example, the η meson has decays to $\gamma\gamma$, $\gamma e^{+}e^{-}$ and $\gamma\mu^{+}\mu^{-}$. These ratios for these three decays can be affected by the splitting kernel of the VINCIA shower, which describes the probability of a photon splitting into a pair of fermions, such as an electron-positron pair. We would like to have a look out how this splitting affects the ratio of the three decay modes and whether the ratio is inclusive or exclusive of these splitting effects. Similarly we would like to include the effects of vector meson dominance [34, 35, 36], this phenomenon is caused by the photon splitting to a pair of quarks, where the photon can then interact as a vector meson. This mixing between vector mesons, such as the ρ^{0}, can affect the possible decays since for example a ρ^{0} can decay to a pair of pions which a photon can not directly decay to. A similar treatment could be used as in VINCIA's electroweak shower [37], where instead of modelling the emission of a photon we model the emission of a ρ^{0}.

8 Conclusion

In conclusion we have implemented a novel approach to QED radiation off of hadron decays, through using the Vincia parton shower. This method differs from other methods by being a parton shower rather than a pure "after-burner", where radiation is all handled after the decay process. This approach seems to replicate the results of existing methods such as PHOTOS quite well, with the advantages of being internal to VINCIA, such as maintainability and being more easily expandable. In performing our comparisons to Photos, we found that the Vincia implementation radiates more energy for a higher proportion of its events outside of the first bin. Additionally, we found an abnormally large disagreement in the case of a decaying charged hadron, which we plan to look into by considering the analogous decay of the $W^{\pm}$ boson. There are multiple ways we would like to expand on this implementation, such as the addition of a spin-three-halves antenna and form factors.

References

[1] W. T. Giele, D. A. Kosower, and P. Z. Skands, "A simple shower and matching algorithm," *Phys. Rev. D*, vol. 78, p. 014026, 2008.

[2] P. Golonka and Z. Was, "PHOTOS monte carlo: a precision tool for QED corrections in z and w decays," *The European Physical Journal C*, vol. 45, pp. 97–107, jan 2006.

[3] E. Barberio, B. van Eijk, and Z. Was, "PHOTOS: A Universal Monte Carlo for QED radiative corrections in decays," *Comput. Phys. Commun.*, vol. 66, pp. 115–128, 1991.

[4] E. Barberio and Z. Was, "PHOTOS: A Universal Monte Carlo for QED radiative corrections. Version 2.0," *Comput. Phys. Commun.*, vol. 79, pp. 291–308, 1994.

[5] P. Golonka, *Computer simulations in high energy physics: a case for PHOTOS, MC-TESTER, TAUOLA and at2sim*. PhD thesis, Cracow, INP, 2006.

[6] N. Davidson, T. Przedzinski, and Z. Was, "PHOTOS interface in C++: Technical and Physics Documentation," *Comput. Phys. Commun.*, vol. 199, pp. 86–101, 2016.

[7] C. Bierlich, S. Chakraborty, N. Desai, L. Gellersen, I. Helenius, P. Ilten, L. Lönnblad, S. Mrenna, S. Prestel, C. T. Preuss, T. Sjöstrand, P. Skands, M. Utheim, and R. Verheyen, "A comprehensive guide to the physics and usage of PYTHIA 8.3," *SciPost Phys. Codebases*, p. 8, 2022.

[8] J. Bellm *et al.*, "Herwig 7.2 release note," *Eur. Phys. J. C*, vol. 80, no. 5, p. 452, 2020.

[9] E. Bothmann *et al.*, "Event Generation with Sherpa 2.2," *SciPost Phys.*, vol. 7, no. 3, p. 034, 2019.

[10] D. J. Lange, "The EvtGen particle decay simulation package," *Nucl. Instrum. Meth. A*, vol. 462, pp. 152–155, 2001.

[11] M. Thomson, *Modern particle physics*. New York: Cambridge University Press, 2013.

[12] P. Skands, "QFT II lectures." PHS5020 Monash University, 2022.

[13] T. D. Lee and M. Nauenberg, "Degenerate systems and mass singularities," *Phys. Rev.*, vol. 133, pp. B1549–B1562, Mar 1964.

[14] M. D. Schwartz, *Quantum field theory and the standard model*. Cambridge, England: Cambridge University Press, Dec. 2013.

[15] A. J. Larkoski, "An Unorthodox Introduction to QCD," 9 2017.

[16] P. Z. Skands, "QCD for Collider Physics," in *2010 European School of High Energy Physics*, 4 2011.

[17] C. Oleari, "The powheg box," *Nuclear Physics B - Proceedings Supplements*, vol. 205-206, pp. 36–41, 2010. Loops and Legs in Quantum Field Theory.

[18] S. Frixione, F. Stoeckli, P. Torrielli, B. R. Webber, and C. D. White, "The MCaNLO 4.0 Event Generator," 10 2010.

[19] G. Gustafson and U. Pettersson, "Dipole Formulation of QCD Cascades," *Nucl. Phys. B*, vol. 306, pp. 746–758, 1988.

[20] P. Skands and R. Verheyen, "Multipole photon radiation in the Vincia parton shower," *Phys. Lett. B*, vol. 811, p. 135878, 2020.

[21] D. R. Yennie, S. C. Frautschi, and H. Suura, "The infrared divergence phenomena and high-energy processes," *Annals Phys.*, vol. 13, pp. 379–452, 1961.

[22] R. Kleiss and R. Verheyen, "Final-state QED Multipole Radiation in Antenna Parton Showers," *JHEP*, vol. 11, p. 182, 2017.

[23] H. Brooks, C. T. Preuss, and P. Skands, "Sector Showers for Hadron Collisions," *JHEP*, vol. 07, p. 032, 2020.

[24] H. Brooks and P. Skands, "Coherent showers in decays of colored resonances," *Phys. Rev. D*, vol. 100, no. 7, p. 076006, 2019.

[25] A. G.-D. Ridder, M. Ritzmann, and P. Skands, "Timelike dipole-antenna showers with massive fermions," *Physical Review D*, vol. 85, jan 2012.

[26] D. A. Kosower, "Antenna factorization of gauge-theory amplitudes," *Physical Review D*, vol. 57, pp. 5410–5416, may 1998.

[27] E. Norrbin and T. Sjöstrand, "QCD radiation off heavy particles," *Nuclear Physics B*, vol. 603, pp. 297–342, jun 2001.

[28] H. W. Kuhn, "The hungarian method for the assignment problem," *Naval Research Logistics Quarterly*, vol. 2, no. 1-2, pp. 83–97, 1955.

[29] J. Munkres, "Algorithms for the assignment and transportation problems," *Journal of the Society for Industrial and Applied Mathematics*, vol. 5, no. 1, pp. 32–38, 1957.

[30] B. Andersson, G. Gustafson, G. Ingelman, and T. Sjöstrand, "Parton fragmentation and string dynamics," *Physics Reports*, vol. 97, no. 2, pp. 31–145, 1983.

[31] K. Hamilton and P. Richardson, "Simulation of QED radiation in particle decays using the YFS formalism," *JHEP*, vol. 07, p. 010, 2006.

[32] M. Schonherr and F. Krauss, "Soft Photon Radiation in Particle Decays in SHERPA," *JHEP*, vol. 12, p. 018, 2008.

[33] H. Brooks, P. Skands, and R. Verheyen, "Interleaved resonance decays and electroweak radiation in the Vincia parton shower," *SciPost Phys.*, vol. 12, no. 3, p. 101, 2022.

[34] G. A. Schuler and T. Sjöstrand, "The hadronic properties of the photon in gamma p interactions," *Phys. Lett. B*, vol. 300, pp. 169–174, 1993.

[35] G. A. Schuler and T. Sjöstrand, "Towards a complete description of high-energy photoproduction," *Nucl. Phys. B*, vol. 407, pp. 539–605, 1993.

[36] G. A. Schuler and T. Sjöstrand, "Low and high mass components of the photon distribution functions," *Z. Phys. C*, vol. 68, pp. 607–624, 1995.

[37] R. Kleiss and R. Verheyen, "Collinear electroweak radiation in antenna parton showers," *The European Physical Journal C*, vol. 80, oct 2020.